EUROPEAN ORGANIZATION FOR NUCLEAR RESEARCH

CERN/EP 82-75
14 June 1982

THE EUROPEAN HYBRID SPECTROMETER - A FACILITY TO STUDY MULTIHADRON EVENTS PRODUCED IN HIGH ENERGY INTERACTIONS

LEBC-EHS Collaboration

Amsterdam[1]-Brussels[2]-CERN[3]-Madrid[4]-Mons[5]-Nijmegen[6]-Oxford[7]-Padova[8]-Paris[9]-Rome[10]-Rutherford Lab[11]-Serpukhov[12]-Stockholm[13]-Strasbourg[14]-Trieste[15]-Vienna[16] Collaboration

M. Aguilar-Benitez[4], W.W.M. Allison[7], P. Bagnaia[10], P. Bähler[3], L. Barone[10], W. Bartl[16], J.L. Bénichou[3], A. Bergier[3], A. Bettini[8], M. Boratav[9], B. Brooks[7], F. Bruyant[3], E. Di Capua[10], E. Castelli[15], S. Centro[8], G. Chanel[3], P. Checchia[15], D. Crennel[11], P. Dow[3], J. Duboc[9], M. Dykes[3], F. Etienne[14], P. Ferran[3], C. Fischer[11], R. Frühwirth[3], A. Fucci[3], P. Gällnö[3], C. Gelès[3], S. Gentile[3], M. de Giorgi[8], A. Guiard-Marigny[3], D. Gusewell[3], P. van Hal[6], F. Hartjes[1], A. Hervé[3], S.O. Holmgren[13], J. Hrubec[16]*, P.T. Hughes[7], M. Van Immerseel[2], D. Jacobs[3], K.E. Johansson[3,13], J. Kesteman[5], A.G. Kholodenko[12], E.P. Kistenev[12], S. Kitamura[3], W. Kittel[6], P. Ladron de Guevara[4], P. Lecoq[3], H. Leutz[3], J.M. Lesceux[5], T. Lingjaerde[3], C. Ljuslin[3], J.C. Marin[3], M. Mazzucato[8], N.G. Minaev[12], T. Moa[13], L. Montanet[3], G. Neuhofer[16], D. Pascoli[8], G. Passardi[3], M. Pernicka[16], O. Pingot[5], G. Piredda[10], B.F. Poljakov[12], A. Poppleton[3], P. Poropat[15], B. Powell[3], F. Prent[3], M. Regler[16], S. Reucroft[3], L. Robb[11], P. Rossi[8], P.D. Shield[7], A. Stergiou[6], J. Tischhauser[3], D.Z. Toet[1], M.C. Touboul[9], C. Troncon[15], L. Ventura[8], C. Willmott[4], F. Wittgenstein[3], D. Zanello[10], L. Zanello[10], P. Zotto[8] and G. Zumerle[8]*

Submitted to Nuclear Instruments and Methods

(*) Now at CERN.

0905P/KEJ/ed

ABSTRACT

The European Hybrid Spectrometer is described in its preliminary version for the NA16 charm experiment. The performance of the small hydrogen bubble chamber LEBC and the detectors of the spectrometer is discussed. In particular the combination of the bubble chamber information with the spectrometer data is described in detail. The track reconstruction efficiency is 90%. The precision with which vertices seen in the bubble chamber are reconstructed is around 10 μm and the two track resolution is 40 μm. Therefore very complex event configurations, in particular charm particle decays, can be reconstructed correctly.

1. INTRODUCTION

With the main aim of constructing an experimental arrangement which minimizes the systematic effects in the study of complex hadronic final states, it was proposed in 1974 to build a system of particle detectors around a high energy beam at the CERN SPS. This system offers a possibility of determining, with all details, the dynamical features of strong particle interactions and associated weak decays [1,2].

The set-up was designed to have a large geometrical acceptance and good particle identification as well as being flexible enough to adjust its field of view to the observation of unexpected new phenomena. This excluded, for instance, the construction of a huge bubble chamber, and favoured a separation of the vertex detector, which gives the exact topology of the interaction. A spectrometer gives the momenta of the secondary particles, gamma detectors give precise information on the produced π^0's and other detectors provide information on the nature of the secondary particles. These ideas have been realized in the "European Hybrid Spectrometer" (EHS).

In 1979, the set-up was still not complete when it became clear that the parts of EHS already constructed (the spectrometer, the gamma detectors and a prototype version of ISIS, a charged particle identifier) could be used, together with a high resolution vertex detector (LEBC, a rapid cycling hydrogen bubble chamber) to study the production and decay properties of the charm particles. This version of EHS is described in this paper. The experiment is known as NA16.

To determine the decay properties of the charm particles, and in particular their lifetimes three conditions must be fulfilled.

(a) The charm particle decays must be "visualized" with a vertex detector giving a spatial resolution of 50 μm or better.

(b) The decays must be reconstructed with the maximum kinematical constraints to remove ambiguities and reject efficiently the background due to events which topologically mimic the charm decays. This requires a large acceptance multitrack spectrometer, charged particle identification and π^0 reconstruction.

(c) Powerful software must be available to match all the information together and reconstruct the decays.

The NA16 experiment satisfies, to a large extent, these three conditions which are used as the main guide for the organization of this paper. We first describe the experimental arrangement, including the vertex detector, the spectrometer, the prototype ISIS1 identifier and the gamma detectors. We then discuss data acquisition and data analysis. We conclude with an example of what has been achieved with EHS in NA16.

2. EXPERIMENTAL ARRANGEMENT

2.1 The beam

The H2 beam line, which provides EHS with particles, is described in detail elsewhere [3].

The final stage of H2 brings the beam from a focus $\sim$ 70 m upstream of EHS to the vertex detector LEBC. At LEBC the final stage quadrupole provided a beam with a horizontal extension of 2 mm and a slightly divergent beam a few centimetres wide in the vertical.

The beam momentum was 360 GeV/c with a momentum byte $\Delta p/p < 1\%$. The flux was typically 5×10^4 particles during the $\sim$ 2 s spill every $\sim$ 10 s. This low flux was dictated by the number of tracks per picture and by space charge effects in ISIS1.

The beam was provided with a fast kicker magnet system [4] which deflects the beam off the target, thus interrupting the production of secondaries for a number of short intervals during the spill. The operation is adjusted to give two kicks during the sensitive time of the

bubble chamber. The first kick removes the early particles which would enter the bubble chamber just before the pressure minimum and which would produce a background of bubbles; the second kick is started by the interaction trigger and removes particles which would enter the chamber after the desired event. The kick duration is $\sim$ 1.5-2.5 ms with an interval between them which can vary from 0 to 2 ms. The rise and fall times were $\sim$ 20 μs, the maximum repetition rate was 50 Hz. The kicker magnet is also of considerable benefit to ISIS1 by suppressing space charge production while the gas gain is being switched on (see below).

2.2 General layout

The general layout of the experiment is shown in fig. 1. LEBC, the small hydrogen bubble chamber is the central detector complemented by a system of proportional wire chambers (U_1, U_3, W_2) and drift chambers (D_1-D_5, PIC). Two spectrometer magnets (M_1', M_2) serve to determine the particle momenta. ISIS is a large volume drift chamber providing relativistic particle identification by ionization sampling, and IGD and FGD are lead glass calorimeters designed for detection of low and high energy photons respectively.

2.3 The bubble chamber LEBC

The LEBC bubble chamber [5] has a cylindrical chamber body, with 20 cm inner diameter and 4 cm free depth (fig. 2). Track sensitivity is achieved by expanding the 1.1 ℓ volume via a 5 mm thick membrane, which forms the rear flat end of the horizontal cylinder and is supported across its outer surface by a hydraulically driven piston. Scotchlite is glued onto the inner surface of this membrane and particle tracks are photographed in bright field illumination through a 25 mm thick window, which is glued to the chamber cylinder.

In order to realize a "clean" chamber with minimum parasitic boiling, all parts of the body were constructed from Lexan. This thermoplastic polycarbonate has a low elastic modulus and is not brittle at cryogenic temperatures. The chamber cylinder with its 2 mm thick beam windows and the expansion membrane were machined from one single Lexan block. This

basic structure was then vacuum sealed with the Lexan optics window by solvent cementing the two parts along a 30 mm wide annular margin. To avoid light absorption in the optics window, we did not use normal Lexan with its blueish tint, but used a special make(*). All metal-lexan connections required for the heat exchanger, filling valve, pressure transducer and vapour pressure bulb were sealed by a shrinking technique without any glueing.

The LEBC running conditions are summarized in table 1. With a fixed maximum camera frequency of 17 Hz, the choice of 33 Hz for the bubble chamber frequency was determined both by the bubble chamber operation, and the desire to minimize the overall dead time.

A point-like light source of 30 J electrical energy and 30 μs flash duration was installed between the two vertically arranged camera lenses (fig. 2). Its light was guided via two semitransparent mirrors into the liquid hydrogen, as if originating from the two lens apertures. From the Scotchlite, on the inner membrane surface, it was retrodirected into the two lenses, which were of the commercially available Componon-S type(**). With 180 mm focal length and F/11 aperture the optical system has a theoretical resolution of 30 μm with a 3.25 demagnification. The depth of field was 4.4 mm.

Bubble diameters were determined by observing them with a microscope and by scanning across the photographed bubbles with a micro-densitometer. The two methods give very similar results and indicate a bubble diameter in space of (42 ± 6)μm. The rather large error margins indicate that the tracks contain bubbles of different sizes. This is due to the coalescence of bubbles, which depends on the bubble density. From the Poisson-distribution of primary bubbles we find that the counted bubble density (80 cm^{-1}) corresponds to a density at the instant of bubble formation of 97 cm^{-1}.

(*) "Press-polished" optical grade lexan from Westlake Plastics Comp. LENNI, Pennsylvania (USA).

(**) J. Schneider, Optische Werke, D-6550 Bad Kreuznach (Germany).

2.4 The interaction trigger

The interaction trigger (fig. 2) was formed by 2 mm thick scintillation counters upstream and downstream of the bubble chamber. A two millimetre wide beam was defined by the large upstream counters T_1 and T_2 in coincidence with the 2 mm wide finger counter T_3. The veto counter, V, rejected the beam halo and upstream interactions, and the L and R counters served to monitor the beam asymmetry and beam focus, and assured that the main part of the beam enters LEBC in the region of optical focus.

An interaction in the bubble chamber was defined by a coincidence of the two downstream counters, T_4 and T_5, which were placed 5 mm away from the beam centre.

An interaction trigger was thus formed by an incident particle not interacting upstream of LEBC and at least two particles produced in the bubble chamber with a minimum angle with respect to the beam of around 10 mrad in the horizontal plane.

The trigger probability per incident particle was $\sim$ 1.8% for pions and $\sim$ 2.5% for protons corresponding to a 16 mbarn and 22 mbarn cross section respectively. The trigger was designed to be insensitive to elastic and diffractive scattering.

The picture-taking rate was 10-13 per spill and was mainly limited by the film transport time.

Other types of triggers were also available for calibration purposes of a particular device or of the entire spectrometer. In particular incident beam triggers were regularly selected for the spectrometer calibration.

A total of about one million pictures were taken for the NA16 experiment. Around 40% of the pictures had an interaction in the fiducial volume of the bubble chamber.

2.5 The multiwire proportional chambers

Multiwire proportional chambers are used for the incident beam, and in the region close to M_1'. They provide fast and precise information about the beam and the interaction topology.

The two identical beam chambers U_1 and U_3 are placed respectively 35 m and 2 m upstream of the bubble chamber. Their useful area is 26 x 36 cm^2 and they are made of 5 coordinate planes, with wires at angles to the horizontal of: -60°, -60° staggered, 0°, +60°, +60° staggered (in the case of U_1). The 20 µm diameter sense wires, spaced by 2 mm, are stretched on frames of vetronite.

The cathode and sense wire planes alternate with gaps of 8 mm. The cathode planes are made of 100 µm wires, 1 mm spacing and the chambers are enclosed by two 50 µm mylar-aclar foils and two rigid aluminium frames which support the 6 precision pins.

W_2 is a large chamber, covering an acceptance of 1.2 x 2.15 m^2, placed at 1.7 m from the middle of the bubble chamber, in the fringe field of magnet M_1'. It is used for the track match between the bubble chamber and the drift chambers. There are six planes of sense wires with a diameter of 20 µm and spacing of 2 mm at angles of respectively 0°, +30°, +10.9°, -10.9°, -30°, 0° to the horizontal. The cathodes are made of 100 µm wires spaced by 1 mm. All the wires are stretched on vetronite frames 8 or 10 mm thick. Each sense plane is sandwiched between two cathode planes and mylar foils to keep them as independent as possible. The chambers are flushed with a mixture of argon (72%) isobutane (23%), fréon (1%) and methylal (4%).

All the chambers are read out with the RMH system (Receiver Memory Hybrid modules) allowing non-destructive fast read-out [6].

The plateau curves indicate efficiencies exceeding 99.5% for U_1 and U_3 at 5 kV and for W_2 at 4.5 kV, with a strobe width of 200 ns.

2.6 The drift chambers

The spectrometer contained five planar drift chambers with sensitive areas of 4.25 x 2.10 m^2 (D_1-D_3, designed and constructed at the High Energy Physics (H-)Department of the NIKHEF Institute, Amsterdam) and 1.3 x 2 m^2 (D_4, D_5, designed and constructed at the Institute of High Energy Physics of the Austrian Academy of Sciences, Vienna). The larger chambers (D_1-D_3) were intended for the first lever arm, and the smaller chambers (D_4, D_5) were intended for the second lever arm, but for this first version of EHS their positions were somewhat modified (fig. 1).

2.6.1 Construction details

Each drift chamber module consists of four coordinate planes with wire angles of approximately +16.7°, +5.7°, -5.7°, -16.7° with respect to the horizontal plane. These angles were chosen to meet the condition of the butterfly configuration [7]. The butterfly configuration was determined to minimize the ambiguities in point reconstruction. For this configuration the distance between consecutive sense wires vary from plane to plane, in such a way that the distances between the sense wires along the frame are all identical. This distance is 48 mm. The configuration of the drift cell, in a plane normal to the wire direction is given in fig. 3.

For the big chambers each coordinate section consists of four planes: two field shaping wire planes, one sense plus field wire and one spacer plane. The distance between two neighbouring sense wire planes is approximately 40 mm.

The sense wires (gold plated tungsten, diameter 20 μm) were stressed with 50 gf on a winding machine. Positioning of these and the field wires was done by means of a microscope mounted on an accurately aligned rail covering approximately two pin distances (192 cm) at an accuracy < 30 μm.

The field shaping wires (copper-beryllium, diameter 80 μm) were stressed with 300 gf (these data also hold for the field wires) and positioned with respect to the precision-ring based fiducial marks at an

accuracy < 0.1 mm. The field shaping wires were connected to a voltage divider chain to create the graded field. The voltage at each side of the field wire was somewhat more negative to sweep ionization electrons from the "dead" corners of the cell. The field shaping wires close to the sense wires were grounded.

All four coordinate planes of the module were contained in one big gas volume of approximately 2000 ℓ. This gas volume was sealed at both faces of the module by transparent mylar-aclar foils of 50 μm thickness. This arrangement allowed an easy inspection of the whole chamber volume.

For the smaller drift chamber an epoxy-glass fibre construction was used with five independent frames for each coordinate plane. Each coordinate plane of the chamber consists of one central part with sense and field wires sandwiched with the frames for the field shaping wires, A plane is closed with a window foil of aluminized mylar (50 μm mylar, 15 μm aluminium). In this way each plane becomes an independent detector. The spacing between each plane is 40 mm. This modular system has several advantages during building, testing and running, as well as during maintenance.

For optimal space resolution the drift chambers have to be constructed with maximum geometrical accuracy. Peripheral equipment has been constructed with which we obtain an accuracy over the whole length of 2 m, of better than 75 μm with respect to reference pins for the 8 planes produced up to now.

2.6.2 Electronics

We use a modified version of the CERN 4-channel preamplifier discriminator (type 4242) equipped with an MC 10101 line driver. Via flat cables four cards are connected to patch panels which bundle 16 channels each to be connected to a Drift Time Recorder. Further details can be found in ref. [8].

2.6.3 Chamber characteristics

The gas used in the chambers consisted of 50% argon, 49% ethane and about 1% ethylalcohol. The ethylalcohol has been added to prevent steady current at high beam intensities.

Averaged operational voltages for the big drift chambers are -3060 V for the drift field and +1425 V for the sense wires (exact values depend on the wire angle or drift path). For the small chambers these values are -2700 V and +1600 V respectively. A space point reconstruction efficiency of 98% was obtained. The mean drift velocity is 47 μm/ns and 53 μm/ns for the big and small chambers respectively.

2.7 The proportional inclined chamber

The proportional inclined chamber (PIC [9]) is located immediately behind the magnet M_1', 3.7 m downstream of LEBC (fig. 1).

It is a multiwire proportional chamber inclined with respect to the average direction of the tracks, where the drift times are measured. The inclination angle was 28.6° (the maximum allowed by the available space). At this angle almost horizontal tracks give hits on about five adjacent sense wires. By measuring the drift times of the electrons produced in the ionization process several independent measurements of the particle trajectory are obtained.

PIC has one plane of horizontal sense wires with 2 mm pitch between two 8 mm wide gaps. The frames, bigger than the sensitive region to avoid secondary interactions, are 2 m vertically and 0.92 m horizontally. The sensitive area is 0.77 m vert. x 0.624 m hor.

The anode plane consists of W-Au 20 μm diameter sense wires spaced by 2 mm, stretched in frames of vetronite. To achieve high precision in the wire positioning, 15 μm wide 15 mm long grooves were cut in a tin film, previously deposited on the printed circuit. The accuracy in positioning as measured on the bench was ± 3 μm. The high-voltage planes were made by stretching Cu-Be 100 μm wires on vetronite frames. The chamber was closed by two 50 μm mylar-aclar foils on two vetronite frames. Two rigid inox frames, which support four precision pins, completed the chamber. The chamber was flushed with 70% Ar, 30% Isobutane gas mixture.

The electronics consisted of standard CERN preamplifier type 4237, especially designed amplifier-discriminators [10] placed near to the chamber and drift time modules [11], that give the drift time determination within ± 3.4 ns maximum error and the pulse length measurement within ± 6 ns maximum error.

In fig. 4 the measured drift times are plotted as a function of wire numbers for some tracks belonging to the same event. The tracks give rise to V-shaped clusters. Two tracks so close that the V clusters overlap result in a W-shaped cluster (fig. 4(b)). When the two tracks are even closer the cluster looks like the one in fig. 4(c). The presence of two short drift times is an indication of two close tracks. The minimum two track separation is 300 μm, corresponding to an angular separation of 76 μrad for tracks originating from the bubble chamber.

With PIC one obtained:

- a spatial resolution of 100 μm,
- a rough measurement of the angle of the track element (± 1.5°),
- a two-track resolution of 300 μm.

2.8 Spectrometer magnets

Two spectrometer magnets, M_1' and M_2 were used in the experiment. Both are conventional C-magnets with racetrack coils with gaps 40 cm (horizontal) by 110 cm (vertical). The lengths are 100 and 200 cm respectively and the integrated fields are 1.6 and 3.1 Tm.

The measured magnetic field was fitted with polynomials of degree five. The magnet volume was divided into smaller boxes, and for each box the field components were expressed as linear combinations of GRAM polynomials [12]. This approximation gives r.m.s. values of the residuals of about 15 G for each of the three field components.

2.9 ISIS

ISIS is a large volume drift chamber which provides relativistic particle identification by sampling the ionization of each track many times for a large number of tracks simultaneously. It was the first such chamber proposed [13]. The theory of the technique has been reviewed elsewhere [14]. Before the installation in the EHS, ISIS1 was tested in a particle beam at NIMROD [15].

Fig. 5 shows a diagrammatic section of ISIS. The single sense plane comprised of alternate anode and cathode wires is perpendicular to the plane of the figure. Secondaries, non interacting beam tracks and much of the beam halo deposit tracks in the form of free electrons in the large 2 m x 4 m x 1.3 m fiducial volume. These tracks then drift under the influence of the uniform field towards the sense plane. Hits are recorded in the form of wire-number/drift-time/pulse height triplets. The electronics have been described elsewhere [16]. The third coordinate is not measured in ISIS. Details are given in table 2.

ISIS1 was operated at 100 kV. At this voltage breakdown is avoided at the expense of a longer drift time and greater susceptibility to space charge effects. To minimize the latter the anode wire/cathode wire amplification voltage is switched low until 2 ms before each gate defining the sensitive time of the bubble chamber during which the trigger is enabled. The anode/cathode voltage was increased to the "gas amplification ON" value, with the preamplifiers disabled. After a setting time of many time-constants (150 μs) the preamplifiers are reenabled. After the end of the gate the sequence is reversed. In this way with LEBC running at 30 Hz the duty cycle for production of space charge was reduced to about 10%. This technique which worked well has since been improved for the operation of ISIS2.

A two dimensional picture of the tracks passing through the drift space is obtained by plotting the drift time against the channel number for all hits. Indeed a hardware display working in parallel with the buffer memory provides such a real time picture direct from the electronics during the run. A typical picture is shown in fig. 6.

2.10 The gamma detectors

The gamma detection is performed by two electromagnetic calorimeters, both using lead-glass blocks to absorb the electromagnetic showers. The first is the Intermediate Gamma Detector (IGD), situated just upstream of the magnet M_2 at about 10 m from LEBC. The Forward Gamma Detector (FGD) is installed at the end of the spectrometer (roughly 35 m downstream of LEBC).

The IGD is a single matrix of 1122 lead-glass blocks, each 5 x 5 x 42 cm^3 (about 15 radiation lengths in depth). It consists of 39 columns and 32 rows of blocks with a central hole (to allow the charged particles to reach the second lever-arm) (fig. 7). Thus the surface covered by IGD is 195 x 160 cm^2 with a hole of 35 x 90 cm^2. Its design was optimized to have a good reconstruction efficiency for π^0's with $x_F > 0.05$ and energies up to 20 GeV (for larger energies the resulting electromagnetic showers are only partially absorbed). The light collected in the lead-glass blocks is used for simultaneous energy and coordinate reconstruction.

The FGD covers the image of the IGD hole at the end of the spectrometer. It consists of a photon converter wall of lead-glass blocks 15 cm thick (4.7 radiation lengths) a hodoscope with three planes of PLEXIPOP scintillator oriented at 45° from each other (for a total of 375 "fingers" each 1.5 cm wide) to measure the shower position, and of an absorber wall of 112 lead-glass blocks, 15 x 15 x 60 cm^3 (24 radiation lengths in depth) for the central 8 x 8 matrix, and 15 x 15 x 40 cm^3 for the upper and lower regions (fig. 8). The total surface covered by the FGD is 120 cm wide and 210 cm high. The FGD was designed to detect the highest energy π^0's hence the difference in conception with the IGD.

Both detectors are mounted on stages with two-dimensional displacement allowing each individual counter to be placed in an electron beam to be calibrated. Both detectors are monitored (to detect and measure instability in the individual counters) with the help of a laser (used as a central light source) and a light distribution system through optical fibres.

A series of runs in monoenergetic electron beams have given the following performance for the two gamma detectors: energy-resolution $\frac{\Delta E}{E} = \frac{0.15}{\sqrt{E}} + 0.02$ (FWHM) for IGD between 2 and 40 GeV, and for FGD. These values are probably overestimated since they include the electron-beam energy-dispersion. The spatial resolution was found to be (for single electron showers) ± 3.5 mm in IGD (for 5 GeV electrons) and ± 2.5 mm in FGD (for 50 GeV electrons). Further information on data processing, shower recognition, π^0 reconstruction efficiency, etc. is given in sect. 4.4. Further details of the gamma detectors are found in ref. [17].

3. ON-LINE COMPUTING

The variety of equipment to be installed at EHS, and the need to allow for future expansion, dictated the use of a multi-branch CAMAC system. This was implemented with a GEC-Elliot CAMAC System Crate. The large number of people involved and the different aspects of the installation, testing and running of this equipment made it desirable to have a computer whose operating system supported multi-tasking foreground, virtual memory and multi-user background. A loosely-coupled dual system manufactured by NORSK DATA was chosen: for data acquisition and data monitoring, an ND10S with two 10 megabyte disks and two 1600 bpi, 75 ips tape units and for equipment monitoring a smaller ND10S configuration.

3.1 Data acquisition and data monitoring

The data acquisition system was based on the CERN standard package for ND computers [18]. This consists of circular buffering of data between producer tasks reading from CAMAC and consumer tasks doing output or online analysis. The CAMAC input to the buffer, and the magtape writing from it, are performed by standard, highly optimized tasks; lower priority monitoring programs can access samples of physics events from the circular buffer.

At EHS the path of physics data to tape is called the Main Chain and is controlled from a dedicated terminal.

The package was greatly extended to allow concurrent, independent data monitoring for each detector by different "subsystems". A subsystem deals with one detector, or detector type, only and is implemented as a suite of four realtime programs:

(a) Operator Communication handles dialogue with the subsystem user via one of several terminals.

(b) Data Input furnishes the data to be used in the subsystem test. This may be physics data from the circular buffer of the Main Chain, or data read on a private basis from the subsystem's detectors during the 10 s or so which separate beam spills. The source of the private data may be various electronic tests, LED calibration pulses for photo-multipliers, etc. and is generally proper to the subsystem and independent of the rest of the spectrometer.

(c) Data Analysis selects physicist-specified subsets of the data, performs calculations and builds histograms.

(d) Data Display outputs these histograms and results of tests to the physicist.

All subsystems may be active at the same time and may carry out their tasks of data validation, detector re-calibration and data-channel monitoring while data recording continues undisturbed in the Main Chain. In NA16 subsystems were implemented for wire chambers, drift chambers, gamma detectors, trigger and ISIS1.

Physicist interaction with the main chain and with each subsystem is via a specially developed commanded handler which allows selection by name or tree-structured menu and can autonomously execute lists of commands stored on disc file. Use of the command handler package greatly contributed to the establishment of uniform user interfaces to the various subsystems.

The throughput of the system was limited by a combination of tape-writing speed and buffer size in computer memory so that for NA16 a maximum of about 160 Kbytes could be recorded per spill. In fact the event rate was normally trigger limited for all but the highest-intensity spills. On average about 10 events with a mean size of 6.8 Kbytes were recorded per spill. A typical event took some 14 ms to read from CAMAC, including a 1.5 ms wait for ISIS data conversion, with a further 2.8 ms for re-initialisation. The readout deadtime was thus much less than that due to the bubble chamber cameras.

3.2 Equipment monitoring and control

Constant monitoring of high voltage levels, etc. is required to maintain the optimal performance of each detector, and this is provided by the second ND10S.

Central to the monitoring system is a specially designed database containing expected values and tolerances. This database has been written to make direct use of the paging and virtual memory capabilities of the ND10S and is free of disc file system overheads. Several limited-intelligence scanning functions have been distributed to front-end microprocessors. Only when a deviant value is detected by a microprocessor is the N10S activated. For high precision monitoring of analog signals, a 1000 channel multiplexer has been developed. For other general-purpose monitoring and control functions the SPS-MPX system is used. For quick implementation of monitoring and control tasks during the development phase, the NODAL [19] system has proved to be a very powerful tool.

4. DATA ANALYSIS

4.1 Introduction

For this type of hybrid experiment, the data are composed of parts which have very different characteristics, namely the bubble chamber photograph and the spectrometer data. The bubble chamber photograph contains very detailed information of the event configuration, and the

tracks in the vertex region are very precisely determined. However, the forward jet of particles often gives rise to ambiguities due to the different ways the two bubble chamber views can be combined.

In the spectrometer, i.e. in the proportional wire chamber and the five drift chambers, the different tracks are easily resolved. The tracks are, however, not determined with the same precision as in the bubble chamber. The identity and energy of the neutral particles are determined with the two gamma detectors.

The aim of the data analysis is for the charged particles to reconstruct the tracks in the bubble chamber and in the spectrometer and to find the correspondance between the tracks and hence their momenta. This "hybridization" process is complicated by the presence of a magnetic field between the bubble chamber and the spectrometer, and is performed in several steps.

First the position and performance of all detectors have to be determined and constantly monitored.

Second the bubble chamber photos must be scanned. The upstream wire chambers U_1 and U_3 give a scan table coordinate prediction for the interacting beam track.

Third the bubble chamber measurements and spectrometer data have to be matched precisely to determine the particle momenta.

4.2 The spectrometer alignment

For a successful hybridization of the tracks, it is important to know very precisely the positions of the chambers and the drift parameters of the drift chambers. The geometer survey data are accurate enough for most of the components (BC, magnets, GD, ISIS, upstream small beam chambers). For the large downstream chambers an accurate calibration is needed. The program SURVEY has been written to find the positions and drift parameters by making use of "beam-through" track data, accumulated at regular intervals during the run.

The technique used is the following: a local system is defined by the central wires of two planes in each of the upstream proportional chambers (U_1, U_3). The relative radial positions of all planes of U_1 and U_3 (whose wire directions are given by the survey measurement) are obtained iteratively by fitting straight lines through the hits recorded for a sample of beam tracks. About 600 tracks are needed to get the required accuracy (10 μm). The local system is transformed into the EHS reference system and the radial positions of all wire planes are expressed in that unique system.

The beam tracks are also used to determine the parameters of the large downstream chambers. Tracks obtained by the straight line fit upstream are swum through the magnets M_1' and M_2 up to the position of each downstream plane. The predictions are compared with the hit positions computed from the real data. For the proportional chamber W_2 the same approach is used as for U_1, U_3. For the drift chambers the very short drift time signals (left-right ambiguities close to the sense wires) and the very long drift-times (non-linearity close to the field wires) are discarded. The plots of the predicted radial position in a drift cell, versus the "recorded" time give the typical V-shape structure as shown in fig. 9. The slope of the arms gives the drift velocity, the intercept of the two arms projected onto the horizontal axis give the zero drift time, the same intercept projected on the vertical axis gives the correction to the radial position of the wire plane. About five iterations are needed to obtain stable parameters with the required accuracy. After convergence a curve is fitted, quadratic in drift time, to absorb non linearities of the apparent drift velocity.

4.3 The track reconstruction

4.3.1 Tracks going through the complete spectrometer

First those tracks which are fast enough to enter the second lever arm of the spectrometer are reconstructed (program GEOHYB). They are usually sufficiently constrained to be filtered out unambiguously. Impacts are reconstructed in the second lever arm. All pairs of impacts in D_1 and D_5 which can be combined to give track candidates coming from any one of the bubble chamber vertices (i.e., pointing close to a vertex in the non-

deflection plane, and having a reasonable impact parameter to that vertex in the deflection plane) are used. Their parameters are obtained by a straight line fit to the hits in all planes of the two chambers. For each track candidate, assuming that the point from which it originates is the primary vertex (or close to it in the transverse direction), predictions are made for the intercept of the track at the positions of the wire chambers in the first lever arm. At the same time the list of significant scattering media seen by the track is set-up. For each chamber in the first lever arm (W_2, D_4, D_2, D_3) the hits compatible with the prediction in each plane are selected and combined to form impacts in those chambers. If no prediction is satisfied in two consecutive chambers the track candidate is rejected. Conversely it may happen that more than one impact is found per chamber. Those impacts are used to define track candidates in the first lever arm. Each candidate is duplicated when more than one vertex is accepted as a possible origin in the bubble chamber.

Each candidate in the first lever arm is combined with its parent candidate in the second lever arm and a global spectrometer fit is performed which takes into account the multiple scattering and returns the best track parameters (momentum and direction) at the level of the first chamber W_2 in the first lever arm. For each surviving candidate the best approximation of the track parameters (at each possible vertex) with their errors is calculated. The next step is to identify which bubble chamber track images on both views are compatible with the prediction. For each acceptable pair of track images a hybrid fit is performed which makes use of the film measurement in both views on the one hand and of the results of the spectrometer fit on the other hand.

Spectrometer tracks which passed the spectrometer fit and failed the hybrid fit, or spectrometer tracks which have been discarded in the final decision are kept temporarily as "hanging" tracks (which may correspond to fast secondary products originating outside the visible volume of the bubble chamber). All wire hits used by the hybrid tracks are flagged as "used". Then, only the hanging tracks which have a low percentage of wires declared as used are kept.

4.3.2 Tracks going through the first lever arm

Once all fast tracks in the forward cone have been reconstructed, it is easier to reconstruct unambiguously impacts in the first lever arm chambers W_2, D_4, D_2, D_3, discarding impact candidates with too many wires previously flagged as "used". The track candidates in the first lever arm are obtained, starting first with those which can reach D_3, and repeating the same for D_2 and D_4.

For each track candidate a complete hybrid fit is performed using all information compatible with the track. The final result for all hybrid tracks found can be inconsistent and the best solution is then searched for. Any track found in both lever arms (sect. 4.3.1) is reinjected to take part in the final decision process.

4.3.3 Tracks not reaching the spectrometer

The track images which have not been hybridized are used to reconstruct tracks in the bubble chamber. In the absence of field the momentum is not known and the reconstruction is made only when the determination of the track direction can be useful for event identification, for instance at secondary vertices. The limited depth of field is often useful in sorting out ambiguities.

4.3.4 Spectrometer tracks not coming from the bubble chamber vertices

Some tracks reconstructed in the spectrometer come from secondary interactions or particle decays outside the visible volume of the bubble chamber. These must be reconstructed since they may influence the interpretation of the gamma detector data. This work is done in a separate pass of a simplified GEOHYB.

All impacts which can be reconstructed in each chamber (with a large tolerance on the a priori possible track direction and with at least two "unused" wires) are computed. Track segments are then formed and extrapolated to the IGD and the FGD. As these combinations are poorly constrained many candidates are often found. To reduce these, the ISIS geometrical data are used to confirm or to veto the candidates.

4.3.5 Acceptance

The spectrometer acceptance is limited by the M_1' aperture (100 x 40 cm²) and corresponds to an angular acceptance of ∿ 200 x 80 mrad² for tracks originating in LEBC. The IGD dimensions (195 x 160 cm²) correspond to production angles of 95 x 80 mrad² (the FGD covers the central hole completely horizontally, but only 70% vertically). For a beam momentum of 360 GeV/c, particles produced forward in the centre-of-mass hemisphere have a laboratory angle of less than 80 mrad with respect to the beam direction, and forward hadrons will have lab momenta of at least 1.8 GeV/c. M_1' can be crudely approximated by a vertical transverse momentum kick of 0.5 GeV/c at 2 m from the vertex so in the limiting case of a charged pion at rest in the centre of mass the track will leave the spectrometer just after the start of ISIS.

Thus the spectrometer should detect all charged tracks and most γ's with $x_F \geq 0$. For measured events satisfying the NA16 scanning criteria, the fraction of charged tracks reconstructed in the spectrometer was ∿ 55% of those produced in LEBC, and the number reaching the end of the spectrometer was 15%. Fig. 10 shows the momentum distribution for tracks reconstructed as far as ISIS, the end of first and second lever arm. It is clear that the second lever arm acceptance is well matched to the requirement of improved momentum precision above 30 GeV/c. The tail of fast tracks reconstructed only as far as ISIS is explained by the ∿ 2% interaction length of ISIS. The limiting effect of the magnet apertures on the acceptance of each lever arm is evident in the dip angle (angle in non-bending plane) distribution shown in fig. 11.

4.3.6 Residuals and efficiencies

The position information provided by LEBC is more than an order of magnitude more precise than any other device in the spectrometer, residuals to a straight line fit to track measurements are 8-10 μm in space. Angular precision on tracks is limited to ∿ 0.1 mrad by the precision of fiducial mark measurements which are required to transform track measurements from the recording medium (film) to the spectrometer coordinate system.

Line fit residuals in the drift chambers are typically 300-350 μm (r.m.s.) per plane, except for high inclination tracks where they are significantly worse. The precision of an impact reconstructed in a drift chamber (4 planes with sense wires at -16.7°, -5.7°, +5.7°, +16.7° to the horizontal) is thus about 200 μm (1 mm) in the bending (non-bending) planes. Calibration data taken with non-interacting beam tracks show a high efficiency for registering hits outside a region of ∿ 1 mm around each field wire (48 mm wire spacing), with shadowing by other tracks (δ rays) being the main cause of inefficiency. The electronic dead time of ∿ 40 nsec corresponds to a ∿ 2 mm shadow. Overall single plane efficiencies are 97-98% for calibration data, but multitrack shadowing reduces this for event data to below 80% in the most densely populated region before ISIS. Space charge (positive ion) build up in the beam region causes local reductions in the drift velocity of ∿ 1-2%.

The multiwire proportional chamber W_2 situated at the start of the spectrometer is less precise (2 mm wire spacing) than a drift chamber, but has a ∿ 95% single plane efficiency for beam or event data - although it cannot distinguish the number of tracks responsible for any single hit.

4.3.7 Momentum measurement

The momentum (p) of a charged track is measured from its angular deflection (θ) in the magnets M_1' and M_2. The expected angular precision in either lever arm is ∿ 40 μrad from the drift chamber precision (200 μm) and spacing (5 m), in LEBC it is ∿ 100 μrad. Then

$$\frac{\Delta p}{p} = \frac{\Delta \theta}{\theta} = 2.2 \times 10^{-4}\ p\ (\text{GeV/c}) \text{ for LEBC + first lever arm}$$

$$= 0.44 \times 10^{-4}\ p\ (\text{GeV/c}) \text{ for LEBC + both lever arms.}$$

At the beam momentum (360 GeV/c) $\frac{\Delta p}{p}$ = 1.6% when using LEBC and both lever arms.

Below 120 GeV/c the momentum error is dominated by multiple Coulomb scattering in the various media (the largest contributions are from the bubble chamber liquid and exit window, ISIS, and air - there is 7% of a radiation length of air between LEBC and D5).

So

$$\frac{\Delta p}{p} \sim 0.7\% \text{ for } p < 30 \text{ GeV/c (first lever arm)}$$

$$\sim 0.6\% \text{ for } p < 120 \text{ GeV/c (second lever arm)}$$

The error on the production angle is 150 μrad and 60 μrad respectively with approximately equal contributions from the bending and non-bending planes - the greater length available for the latter being compensated by the lower bubble and drift chamber precision in this direction.

4.3.8 Mass resolution

The resolution on the effective mass of a multibody system depends mainly on the momentum uncertainty, the angular error being small.

Away from threshold (for example in the charm region) $\Delta m \simeq (m/2)(\Delta p/p)$ from each contributing particle.

The mass resolution can be checked using the strange particle decays visible in the bubble chamber, the most frequent being $K^0 \to \pi^+\pi^-$ and $\Lambda^0 \to p\pi^-$. We have obtained $\Delta m_{K^0} \sim 2.6$ MeV/c² and $\Delta m_{\Lambda^0} \sim 1.1$ MeV/c² in agreement with expectations.

This investigation of mass resolution can be extended to $\Sigma^+ \to p\pi^0$ decays. Because the decay includes a π^0, the study then involves the relative behaviour of the EHS charged particle momentum determination and the γ detection system. Unfortunately, fully reconstructed such decays are very rare; nevertheless, some $\Sigma^+ \to p\pi^0$ decays have been identified. Our measurements agree with the generally accepted mass of the Σ^+. For fully reconstructed charmed particle decays the mass error is 10-20 MeV/c² according to decay topology. Fig. 12 shows the effective mass of $D^{\pm}$ decays into three charged tracks ($\pi\pi\pi$ or $K\pi\pi$) plus 0, 1 or 2 π^0's the decay being visible in the bubble chamber and the π^0's being identified using the gamma detectors. The Cabibbo favoured and forbidden combinations are shown in figs 12(a) and 12(b) respectively. A peak at the D mass is easily seen for the Cabibbo favoured particle combinations.

4.3.9 Reconstruction efficiency

About 2% of tracks interact in the exit walls of the bubble chamber or the trigger scintillator. In addition tracks may decay before reaching the spectrometer ($\sim$ 5% at 2 GeV/c). Since V^0 decays can be identified when only 1 of the 2 tracks has its momentum measured, the reconstruction efficiency can be estimated using identified V^0's with both tracks expected in the spectrometer. Using pions from identified K^0 decays, fig. 13 shows the momentum distributions for the tracks found in the spectrometer and those expected but not found. Above 2 GeV/c the reconstruction efficiency is $91 \pm 3\%$.

4.4 Particle identification

4.4.1 ISIS1

The raw data collected by ISIS (drift time and pulse height information) is converted into two dimensional track vectors with ionization estimates by the pattern recognition program SPIRES (SPatial and Ionization REconstruction in ISIS). Essentially the pattern recognition procedure consists of three frame scans. In each scan the program starts at one end of the chamber and processes the data wire by wire following all tracks simultaneously. The track segments so created are scanned for pairs that link to form part of the same track although most tracks are reconstructed as a single segment. Tracks that pass through the central sense plane and appear in the data as a "vee" track are linked at this stage.

Once the drift time signals have been spatially classified into tracks, the corresponding pulse heights are histogrammed and fitted by a single parameter maximum likelihood fit as described in ref. [14]. The likelihood function is taken from the observed energy-loss distribution rather than from theoretical calculations. The procedure determines the ionization and its error for each track up to one overall normalisation factor for that roll of film. The latter has to be established by looking at known velocity tracks as discussed below.

To associate the tracks in ISIS with those in the spectrometer the linear transformation between the two is needed. This requires the surveyed position of ISIS on the one hand and the drift velocities and zero drift time on the other. The latter are found using clear cases of association (in NA16 due to a resistor failure in the upper part of the chamber, the two halves were treated separately).

We had intended to use beam tracks to calculate the overall ionization calibration constant. In NA16 this proved impossible due to the space charge problems discussed later. Instead the determination of the constant had to rely on secondary tracks, assumed to be pions, in events with simple topologies at the spectrometer level. Once a spectrometer track with its measured momentum has been associated with a track in ISIS, it is possible to calculate expected ionization values for e, π, K and p mass assignments using the theoretical shape for the relativistic rise [14]. From the fitted ionization and its error, the calibration constant and the expected ionizations, we calculate χ^2 for one degree of freedom for each mass hypothesis. With the limited statistics and systematic effects in ISIS1 particle identification is rarely unique. Both of these are overcome in ISIS2 which is now in operation in EHS [20].

4.4.1.1 Spatial performance

A two dimensional picture of tracks passing through the drift space is obtained by plotting the drift time against the channel number for all hits. A typical picture is shown in fig. 6. A vertical expansion of the lower part of this same picture is shown in fig. 14. In fig. 14(a) the track vectors derived by the analysis programme SPIRES are superimposed while fig. 14(b) shows the vectors of four tracks reconstructed in the bubble chamber and spectrometer overlaid on the data.

The track match efficiency has been calculated using hybridized tracks coming from ordinary events measured in NA16 and tracks reconstructed using only the electronic information from events with simple hit configuration in the first lever arm chambers. The track match statistics are given in tables 3(a) and 3(b). The greater part of the inefficiencies were due to the resistor failure and space charge effects.

The distributions of the mismatch in position and angle between tracks in ISIS1 and the corresponding tracks in the spectrometer are well centred and FWHM spreads are 9 mm and 12 mrad respectively.

The distribution of the separation between neighbouring hits for reconstructed tracks shows that the two-track resolution is 12 mm. The pulse height of hits separated by more than this value showed less than 2% systematic shift.

For the NA16 experiment the beam was only 2 mm wide in the horizontal plane due to the finite depth of field of the high resolution optics of LEBC. As a result, the space charge production was high in this region and the gas gain was found to be lower by 20% for tracks within ± 1 cm if the beam. This effect builds up during the first 200-300 msec of the SPS "flat-top" and distorts the sagittae, spectrometer hooking residuals and pulse heights for such tracks. Tracks in this region are excluded from analysis by ISIS1 in NA16.

4.4.1.2 Pulse heights and particle identification

The particle identification efficiency was studied by considering a sample of well identified tracks. The data described here come from electrons and pions whose identification as well as momenta were established by reconstructing K^0_s decays and γ conversions observed in the bubble chamber. We restrict our sample to decay configurations having two hybridised tracks and giving a unique three-constraint kinematical fit.

Fig. 15 shows the pulse height spectrum for one particular identified electron. Superposed are the predicted spectra for pion, proton and electron. The data clearly discriminate in favour of the electron. In fig. 16 some of the electron and pion fitted ionizations are plotted against momentum. A qualitative separation between pions and electrons and an indication of the log p dependence for pions are observed.

The number of samples available on a track is reduced by the effects of bad channels, overlapping tracks and so on. Taking this into account the expected resolution is 13.8% FWHM. The internal error on the

ionization given by the maximum likelihood fit has a typical value of 14.4% FWHM in agreement with the theoretical value. The validity of this internal error can be checked by considering the distribution of the ratio between the observed and expected ionization for the identified e or π tracks. The width of this distribution is 18.6% FWHM. The discrepancy between 18.6% and 14.4% is of systematic origin (due in part to loss of measured pulse height with drift distance).

In fig. 17 we have plotted the ionization χ^2 for a pion mass against that for an electron mass for the sample of kinematically identified tracks. In general there is good correlation between particles identified by dE/dx and kinematics. With a cut at the 2-standard deviation level we have the results given in table 4. From this table we conclude, in particular, that ISIS1 gives excellent and reliable identification of electrons from hadrons. This has proved important in identifying semileptonic D decays in NA16.

The fraction of tracks that is correctly and uniquely identified is a function of momentum. This is shown in fig. 18. Only a very small number of tracks above 20 GeV/c can be identified by a device with the limited ionization statistics of ISIS1.

Since the completion of NA16 the longer device, ISIS2, has been operated. With a major reduction of both systematic and statistical errors, an ionization resolution of 7.4% FWHM has been achieved for beam tracks [20].

4.4.2 The intermediate gamma detector

The shower recognition procedures are basically different in the two gamma detectors. In the case of the intermediate gamma detector (IGD), the non-zero amplitudes recorded by the individual counters for a multi-shower event are ordered from the highest to the lowest amplitude. A 5 x 5 matrix (25 x 25 cm^2), where the central element is the counter with the highest amplitude, is then assumed to contain a single shower and a consistency check is made on all amplitudes. If the check is satisfactory, the corresponding counters are definitely excluded from any further search.

Otherwise, they are flagged as ambiguous and kept in the list. When there are no more candidates for shower impact counters in the list, an iterative procedure is applied to the ambiguous counters to disentangle overlapping showers. This procedure is generally succesful in separating two showers whose impacts are in two distinct lead-glass blocks (which is the case for most π^0's with energies below 40 GeV). When a single shower is isolated, a maximum likelihood method is used to fit the amplitudes measured in the 9 central counters. Experimental data on the amplitudes as a function of the impact coordinates provide the parameters of a statistical shower model used in the fit. When the fit converges, the fitted energy and coordinates are used as final shower parameters. Otherwise, the sum of the amplitudes gives an estimate of the energy and then the coordinates are computed using a parametrization of the ratios of amplitudes in neighbouring counters. If the fit probability is too low, this is an indication either of the presence of a hadronic shower or of the fact that overlapping showers are being treated as a single one. Fig. 19 shows the ability of this method to recognize as such two electromagnetic showers with energies E_1 and E_2 as a function of their ratio. The points correspond to a 95% probability of recognising as such two showers with a distance Δ between their impact points (the curve is an eyeball fit to the points). The minimum separation distance is about 25 mm for showers of equal energy. When the two photons come from the same π^0, this corresponds to a π^0 energy of around 100 GeV.

4.4.3 The forward gamma detector

The Forward Gamma Detector (FGD) sees the highest energy part of the particle spectrum, therefore a high percentage of photons are close to each other. The problem of resolving them is further complicated by hadrons interacting in the 1.5 absorption lengths that the lead glass represents.

For these reasons, data analysis begins with shower recognition in the hodoscope, which has the finest granularity and is little affected by hadrons, having only one quarter of an absorption length in front of it. Clusters of signals are searched for in each of the three hodoscope planes, and associated using the triangular condition. Combinations not associated with energy in the corresponding converter and absorber blocks are rejected as spurious.

Using the position of each shower, and an empirical parametrization of the lateral development of the shower, a fit is then performed to the energy released in each block, which gives the total energy associated with each hodoscope shower. Since the converter granularity is low, we also use the correlation between the energy release in the converter and the amplitude in the hodoscope: high energy in the converter means early shower development and so high amplitudes in the hodoscope.

It is possible for a particle to release energy in the absorber without giving a sizeable signal in the hodoscope. This is the case for most of the hadrons and for a small part of the photons (2.6%). In this situation, signals in the glass blocks not associated with hodoscope showers are grouped in clusters to form absorber showers. Their energy is the sum of the amplitudes of the relevant blocks, and their position is computed by a weighted average of positions of the same block.

Only for π^0's with energies exceeding 300 GeV, the separation of the two photons is smaller than 3 cm. The lateral profile of a shower in the hodoscope being roughly an exponential of "decay" length 0.9 cm, it is sufficient that they fall on non-adjacent fingers to be distinct in one of the three planes. Showers with a spatial separation of more than 3 cm will therefore always be separated on at least one plane.

If the two photons give rise to very different hodoscope amplitudes, the minimum acceptable separation increases. With an amplitude ratio of five, for example, the minimum separation becomes 3.5 cm. Only 10% of all the combinations have hodoscope amplitudes in a ratio exceeding five. It is worth mentioning that this ratio depends rather weakly on the photon energies, being mainly related to the amount of shower development in the converter.

The analysis of data from the two gamma detectors IGD and FGD is carried out in the program GAMIN which also performs the reconstruction and the fit of the possible two gamma pairs in the π^0 and η region. This procedure is described in more detail in ref. [17].

The $\gamma\gamma$ effective mass distributions of showers detected in the two gamma detectors are shown in fig. 20. The π^0 mass peak is easily seen, and its width is typically 20 MeV/c^2 (FWHM).

5. EXAMPLES OF RECONSTRUCTED EVENTS

5.1 A fully reconstructed K^0_L

Fig. 21 shows an event which demonstrates the simultaneous use of gamma detector and spectrometer information. It is a V^0 which has been identified as $K^0_L \to \pi^+\pi^-\pi^0$. Both of the V^0 charged tracks are successfully reconstructed in the spectrometer yielding particles of momentum 2.1 ± 0.1 GeV/c and 5.8 ± 0.1 GeV/c, respectively. The effective mass of these two particles, assumed as pions, is 321.3 ± 1.5 MeV/c^2 and the resulting combination is not compatible with originating at the primary vertex.

The forward gamma detector FGD has 5 showers and the intermediate gamma detector IGD has 3 showers in this event. These may be associated to give 3 π^0 combinations. If the 8.5 ± 0.3 GeV/c π^0 is associated with the V^0, one obtains an effective mass $M(\pi^+\pi^-\pi^0) = 496 \pm 2$ MeV/c^2. The lifetime is 1.1×10^{-12} s. No other combination of particles gives any recognizable effective mass.

5.2 A beautiful event

Fig. 22 shows a photograph of a proton induced 4-prong event with two neutral particles decaying into two (V2) and four (V4) charged particles respectively. All four tracks of the V4 decay are fully reconstructed and give momenta of 27.2, 8.4, 14.1 and 8.6 GeV/c. If one assumes that these four particles are K^+, π^+, π^- and π^-, respectively one obtains a $\bar{D}^0$ of mass 1865 MeV/c^2 and momentum 58.3 GeV/c. The information from the pictorial drift chamber ISIS1 is consistent with these particle assignments. The $\bar{D}^0$ flight path is 0.42 cm thus giving a proper lifetime of 4.5×10^{-13} s.

Both tracks of the V2 are reconstructed in the spectrometer yielding momenta of 18.4 and 9.1 GeV/c. The 18.4 GeV/c particle is identified by ISIS1 as an e^+ (2.7 standard deviations from the nearest hadron hypothesis); in addition, this particle produces an 18 GeV/c shower in the lead glass wall IGD: The 9.1 GeV/c negative track is consistent with K or π from ISIS1.

The most probable interpretation of this decay is $D^0 \rightarrow K^- e^+ \nu$ and indeed for this hypothesis a kinematic solution can be obtained involving a missing 3 or 33 GeV/c neutrino (two solutions). With this interpretation, the D^0 momentum is 30 or 60 GeV/c and gives a lifetime of 17 or 6 x 10^{-13} s.

6. SUMMARY

The preliminary version of the EHS has demonstrated that complex event configurations can be reconstructed with a good efficiency (track reconstruction efficiency about 90% for particles with momenta exceeding 2 GeV/c).

In particular the decays of strange and charm particles are visualized in the bubble chamber and completely reconstructed combining the bubble chamber information with the spectrometer data. The widths of the reconstructed K^0, Λ^0 and $D^{\pm}$ mass distributions are typically 5, 2 and 30 MeV/c^2 respectively.

Two parameters, very important for the detection of charm particles, namely the two track resolution and the vertex determination are about 40 µm and 10 µm respectively in LEBC.

In the forward hemisphere the lead-glass calorimeters provide π^0 identification, and some charged particle identification is possible in the ISIS prototype.

Acknowledgements

The conception, design, construction and running in of a complex set up like EHS could not be achieved without the effort of a large team of technicians, engineers and physicists. The large contributions from DD and EF Divisions at CERN and from a large number of European laboratories have been essential for this project.

The group from the Institut für Hochenergiephysik, Vienna, wishes to acknowledge the financial support from the Fonds zur Förderung der Wissenschaftlichen Forschung, Vienna, Austria.

REFERENCES

[1] W. Allison et al., The advantages of a rapid cycling bubble chamber for physics at SPS energies, CERN/SPSC 74-45.

[2] W. Allison et al., Study of multihadron events involving identified particles in high energy interactions, CERN/SPS 75-15.

[3] P. Coet, N. Doble and S. Reucroft, Beam possibilities for EHS, CERN/SPS 81-25 (EBP) and refs cited therein.

[4] H. van Brungel and N. Siegel, A pulsed magnet system to modulate the beam for rapid cycling bubble chambers CERN/SPS 81-13 (1981).

[5] J.L. Benichou et al., Nucl. Instr. and Meth. 190 (1981) 487.

[6] J.B. Lindsay et al., Nucl. Instr. and Meth. 156 (1978) 329.

[7] F. Bruyant et al., Nucl. Instr. and Meth. 176 (1980) 409.

[8] G. Daum et al., Nucl. Instr. and Meth, 176 (1980) 119.

[9] M. Pernicka, M. Regler and S. Sychknow, Nucl. Instr. and Meth. 156 (1978) 219-225;

A. Bettini, D. Pascoli and M. Pernicka, Experiences with a Proportional Inclined Chamber in the EHS, submitted to Nucl. Instr. and Meth.

[10] G. Barichello and D. Pascoli, Nucl. Instr. and Meth. 189 (1981) 621-624.

[11] M. Pernicka, Nucl. Instr. and Meth. 156 (1978) 311.

[12] K. Clevermann and F. Louis, Représentation d'un champ magnétique par des polynomes de GRAM, CERN/EP/DHR 77-2.

[13] W.W.M. Allison et al., Nucl. Instr. and Meth. 119 (1974) 499.

[14] W.W.M. Allison and J.H. Cobb, Ann. Rev. Nucl. Part. Sci. 30 (1980) 253.

[15] W.W.M. Allison et al., Nucl. Instr. and Meth. 163 (1979) 331.

[16] C.B. Brooks et al., Nucl. Instr. and Meth. 156 (1978) 297.

[17] B. Powell et al., the EHS lead-glass calorimeters and their laser based monitoring system, to appear in Nucl. Instr. and Meth.

[18] P. Bähler et al., "Clusters of 16/32 bit minicomputers..." Computer Physics Communications 22 (1981) 285.

[19] M.C. Crowley-Milling, G.C. Shering, "The NODAL System for the SPS", CERN 78-7.

[20] W.W.M. Allison, Proc. Int. Conf. on Instrumentation for Colliding Beam Physics, Stanford, California, February 1982.

TABLE CAPTIONS

Table 1 LEBC operating parameters.

Table 2 Description of ISIS1.

Table 3 Track match statistics for ISIS1.

Table 4 Identification statistics for ISIS1.

TABLE 1

Hydrogen temperature	29.1 K
Hydrogen (equilibrium) vapour pressure	7.10 bar
Hydrogen static pressure Hydrogen pressure minimum	8.15 bar 4.10 bar
Hydrogen temperature fluctuations	0.01 K
Piston stroke	1.25 mm
Length of expansion cycle	5 ms
Chamber cycling rate	33 s^{-1}
Camera cycling rate (max.)	17 s^{-1}
Flash delay	300 µs
Beam gate at pressure minimum	800 µs

TABLE 2

Number of channels	80
Max. No. of samples/track	80
Sample size	1.6 cm
Width of fiducial volume	4.0 m
Drift voltage	100/120 kV
Gas mixture	argon/20% CO_2
Multitrack capacity	32/49
Drift time	100 µs
Expected ionization resolution with full no of samples	12% FWHM

TABLE 3

(a) Based on 7567 hybridized tracks

Entering ISIS1 99.3%

Entering upper ISIS1 24.8% of which 68.0% matched uniquely

Entering lower ISIS1 75.2% of which 81.7% matched uniquely

In total 9% of tracks were not matched and 13.2% of tracks were multiply matched.

(b) Based on 42546 hanging tracks

Entering ISIS1 100%

Entering upper ISIS1 20% of which 82.2% matched uniquely

Entering lower ISIS1 80% of which 87.4% matched uniquely

In total 5.2% of tracks were not matched and 8.5% of tracks were multiply matched.

TABLE 4

	Known pions	Known electrons
Total	81	46
Uniquely correct	49 (60%)	17 (37%)
Uniquely wrong	0 (0%)	5 (11%)
Ambiguous	28 (35%)	23 (50%)
Inconsistent (5% expected for cut at 2 s.d.)	4 (5%)	1 (2%)

FIGURE CAPTIONS

Fig. 1 Schematic layout of the experimental arrangement.

Fig. 2 Horizontal section of LEBC in its vacuum tank with the optical arrangement. The scintillation counters which define the incident beam (T_2, T_3, L, R, V) and the trigger (T_4, T_5) are also shown.

Fig. 3 Configuration of a drift cell for a big drift chamber (D_1-D_3).

Fig. 4 Recorded drift times as a function of wire number for PIC.

(a) One track;
(b) Two slightly overlapping tracks;
(c) Two very overlapping tracks.

Fig. 5 A vertical section of ISIS parallel to the beam plane.

Fig. 6 ISIS1 picture from a typical event. The vertical coordinate is the drift time representing the 2 x 2 m drift dimension; the horizontal coordinate is the channel number representing the distance in the beam direction (1.28 m). Certain channels are missing. The wandering tracks are due to very low energy electrons.

Fig. 7 A drawing of the Intermediate Gamma Detector (IGD).

Fig. 8 The arrangement of the lead glass blocks and scintillator hodoscopes of the Forward Gamma Detector (FGD). The detector is seen from the side.

Fig. 9 Transverse coordinate in a drift cell versus the recorded time.

Fig. 10 Momentum distribution for tracks reconstructed as far as ISIS1 (broken line), the end of first lever arm not going through the second lever arm (full line) and using the complete spectrometer (hatched).

FIGURE CAPTIONS (Cont'd)

Fig. 11 Dip angle distribution for tracks reconstructed as far as ISIS1 (broken line), the end of first lever arm not going through the second lever arm (full line) and using the complete spectrometer (hatched).

Fig. 12 (a) Effective mass distribution for 3-prong $D^{\pm}$ decays with Cabibbo favoured combinations ($K^{\pm}\pi^{\mp}\pi^{\mp}n\pi^{0}$, n = 0, 1, 2). There are on the average four combinations per event.

(b) Effective mass distribution for 3-prong $D^{\pm}$ decays with Cabibbo forbidden combinations ($\pi^{\pm}\pi^{\pm}\pi^{\mp}n\pi^{0}$, n = 0, 1, 2). There are on the average about eight combinations per event. All curves are hand drawn eye-guides.

Fig. 13 Momentum distribution for tracks found in the spectrometer and those expected but not found.

Fig. 14 (a) Part of a typical ISIS1 event in the NA16 experiment. The vertical coordinate is the drift dimension; the horizontal coordinate is the channel number representing the distance in the beam direction (1.28 m). Certain channels are missing. The wandering tracks are due to very low energy electrons. The results of ISIS pattern recognition have been superposed.

(b) The same ISIS1 event is shown but with four predictions from the spectrometer superposed.

Fig. 15 Pulse height distribution in ISIS1 for an individual track known to be an electron from its association to a γ conversion in the bubble chamber, The curves are the expected distributions for e, π and protons.

Fig. 16 Plot of observed ionization in ISIS1 against momentum for tracks identified in the bubble chamber and spectrometer as pions or electrons.

FIGURE CAPTIONS (Cont'd)

Fig. 17 (a) Ionization χ^2 for pion versus χ^2 for electron for the sample of tracks known to be electrons in ISIS1. The broken lines mark the 2 standard deviation limits.

(b) As (a) but for kinematically identified pions.

Fig. 18 Identification efficiency for ISIS1 for π/e sample using a 2 standard deviation cut as a function of track momentum.

Fig. 19 Separation of two electromagnetic showers in the gamma detectors as a function of the ratio of these energies.

Fig. 20 The effective mass distributions of showers detected in the IGD alone (a), in the FGD alone (b) and in both detectors (c).

Fig. 21 A photo of an event with a fully reconstructed K_L^0.

Fig. 22 A photo of a 4-prong event with two neutral decays (V2, V4), identified as decays of neutral charm particles.

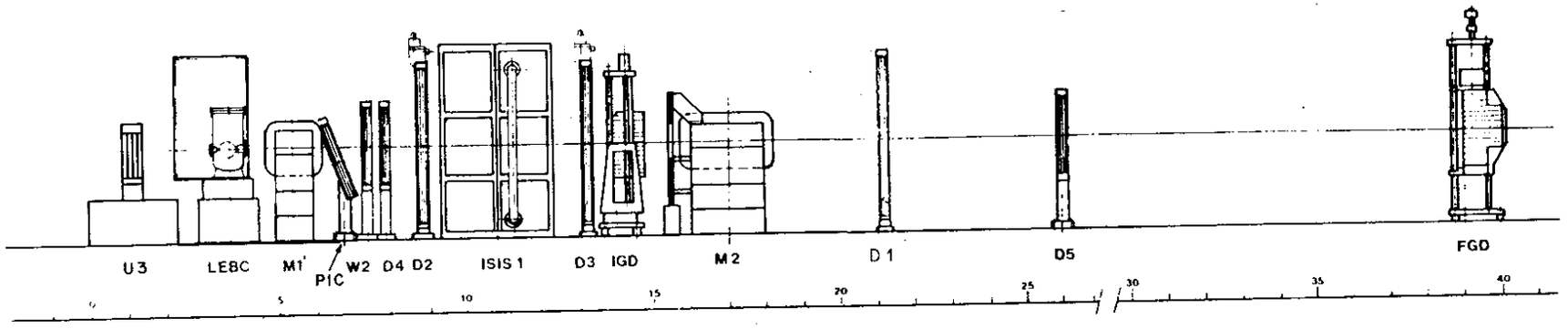

U3, W2	Proportional wire chambers
D1-D5	Drift chambers
PIC	Proportional inclined chamber
IGD, FGD	Lead glass calorimeters
ISIS1	Pictorial drift chamber with ionization sampling
M1,M2	Spectrometer magnets

FIG. 1

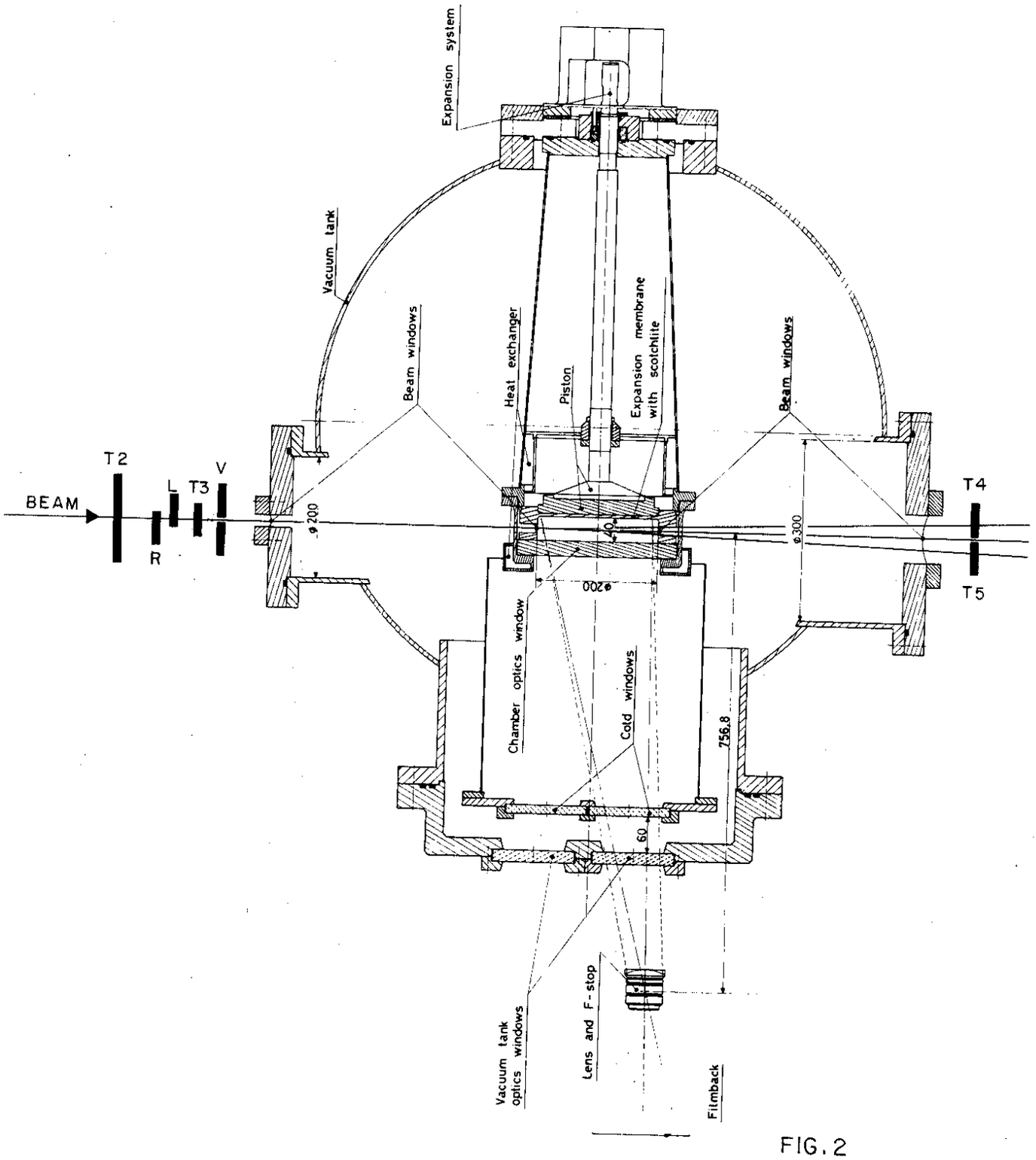
Expansion system
Vacuum tank
Beam windows
Heat exchanger
Piston
Expansion membrane with scotchlite
Beam windows
T2
BEAM
L
T3
V
R
T4
T5
φ200
φ300
φ200
Chamber optics window
Cold windows
756.8
60
Vacuum tank optics windows
Lens and F-stop
Fitmback

FIG. 2

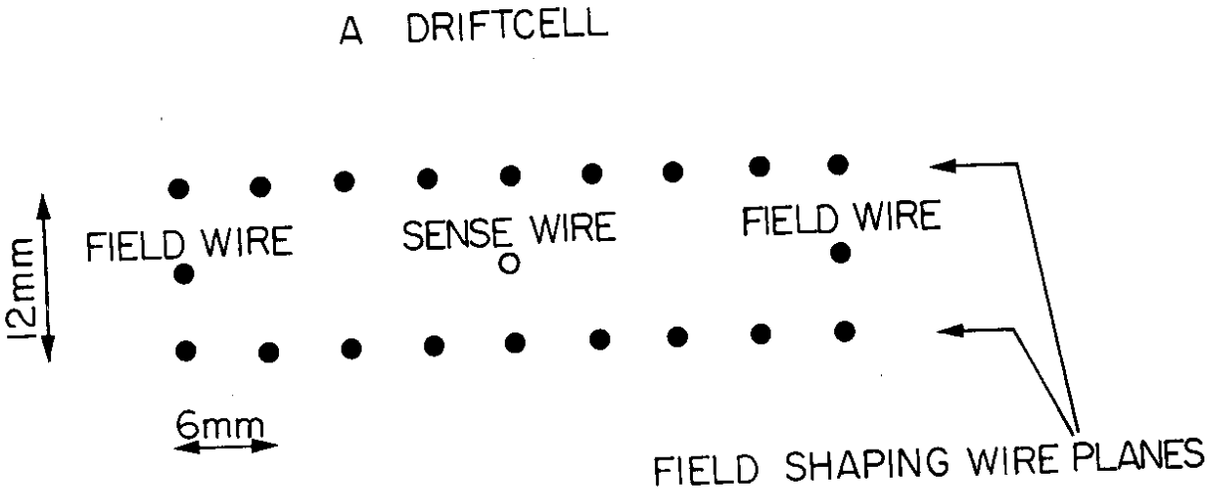
A DRIFTCELL
12mm
FIELD WIRE
SENSE WIRE
FIELD WIRE
6mm
FIELD SHAPING WIRE PLANES

Fig. 3

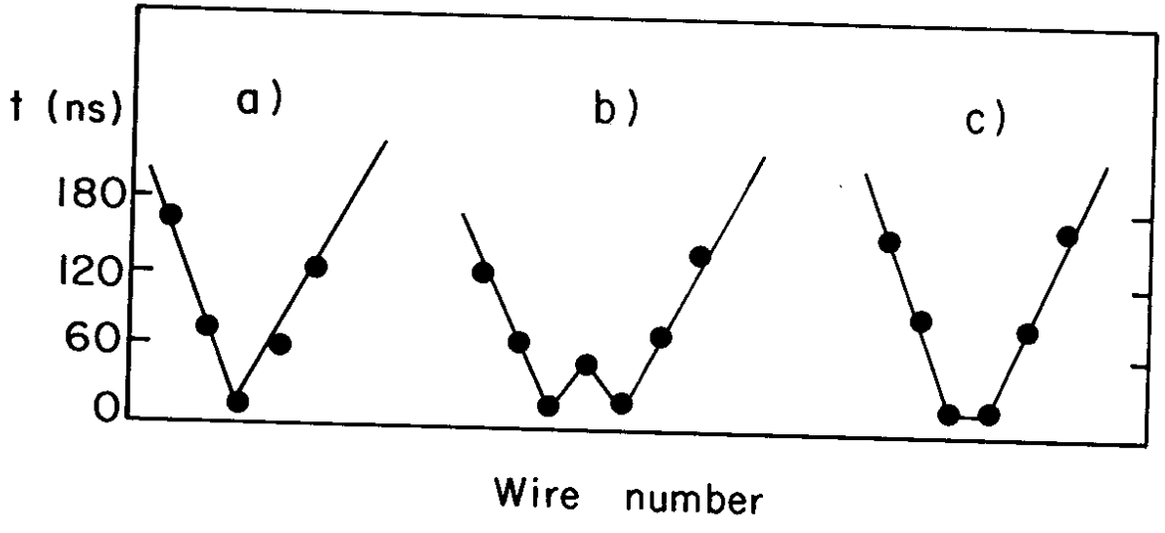

FIG. 4

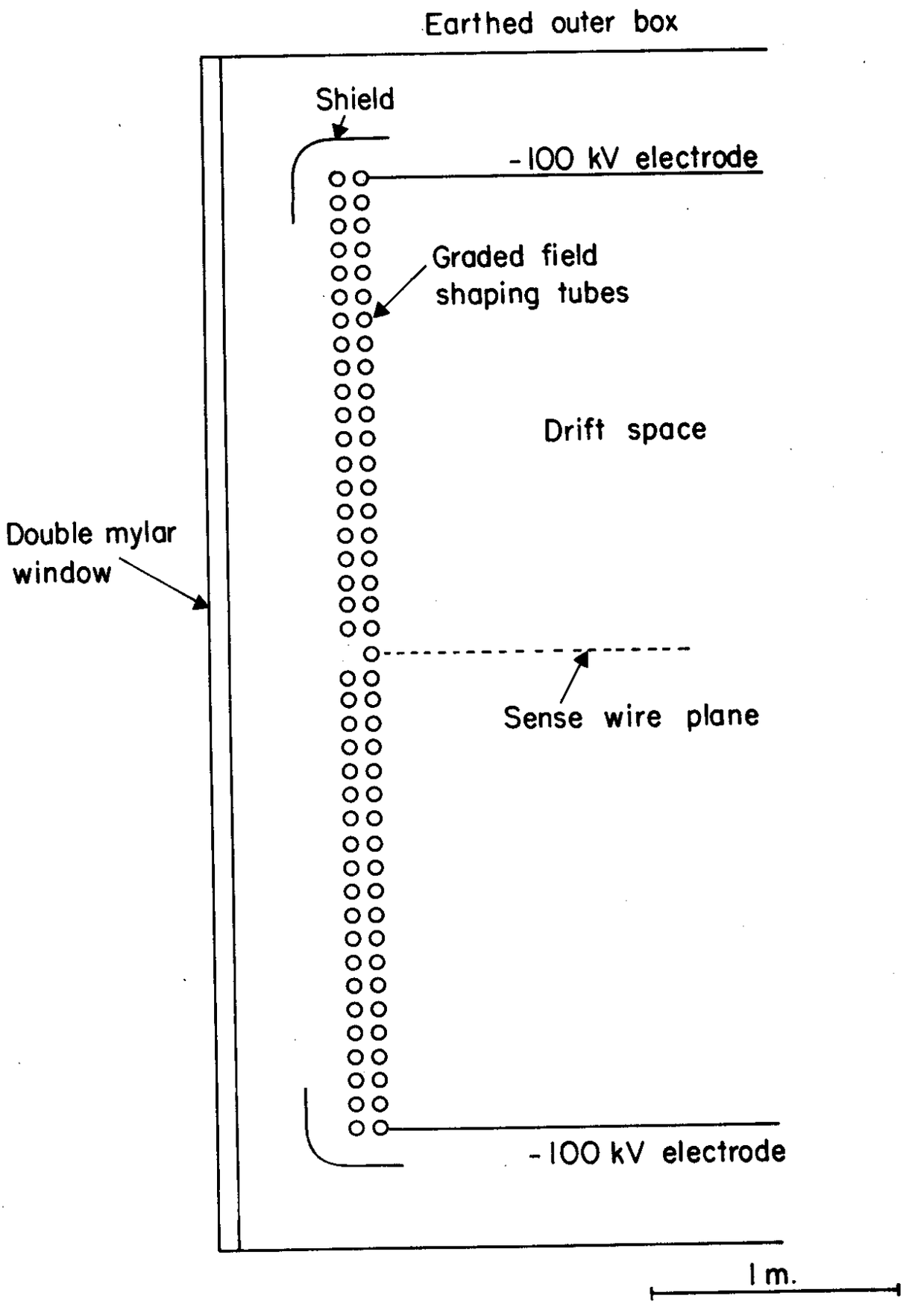
Earthed outer box
Shield
-100 kV electrode
Graded field
shaping tubes
Drift space
Double mylar
window
Sense wire plane
-100 kV electrode
1 m.

FIG. 5

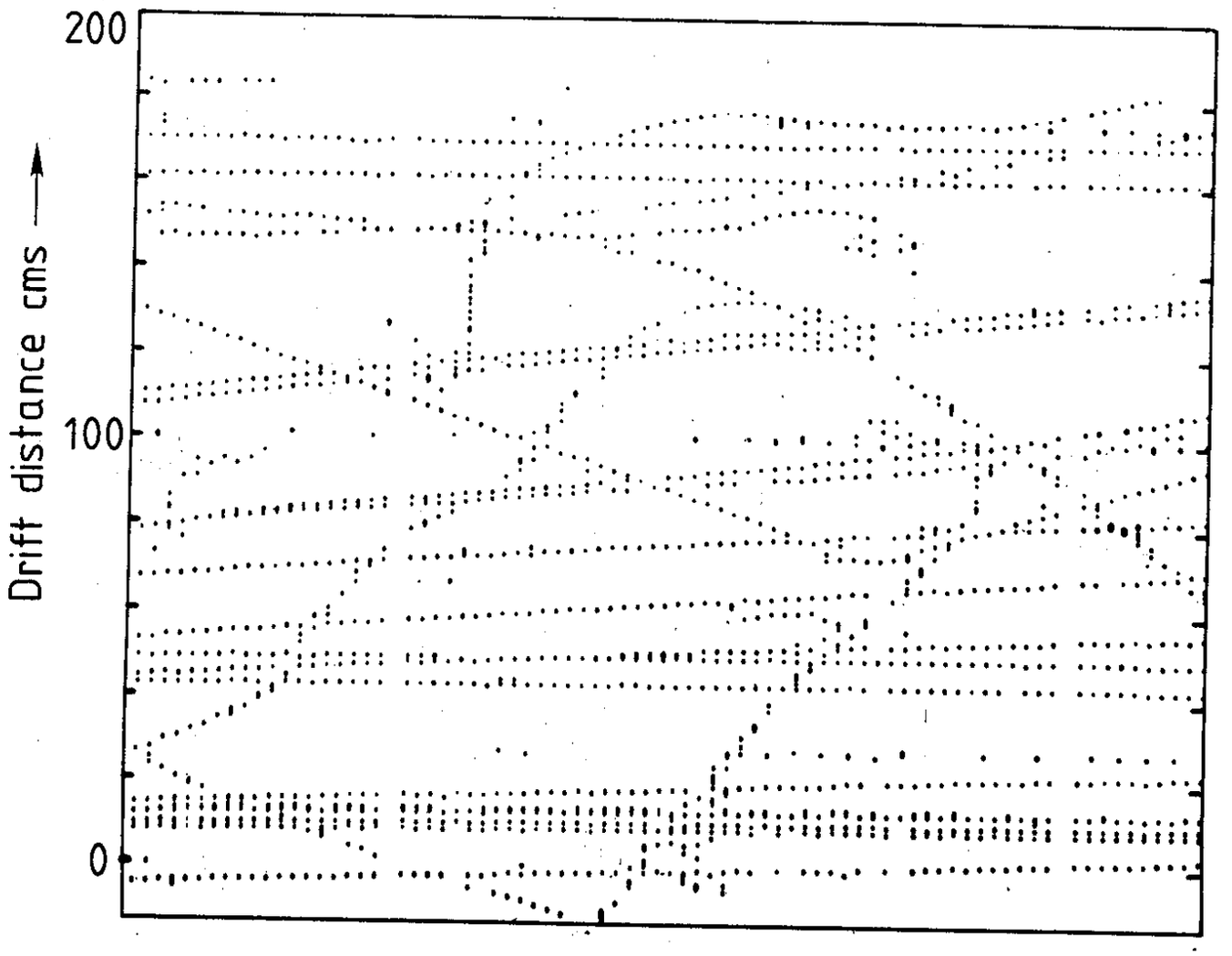

FIG. 6

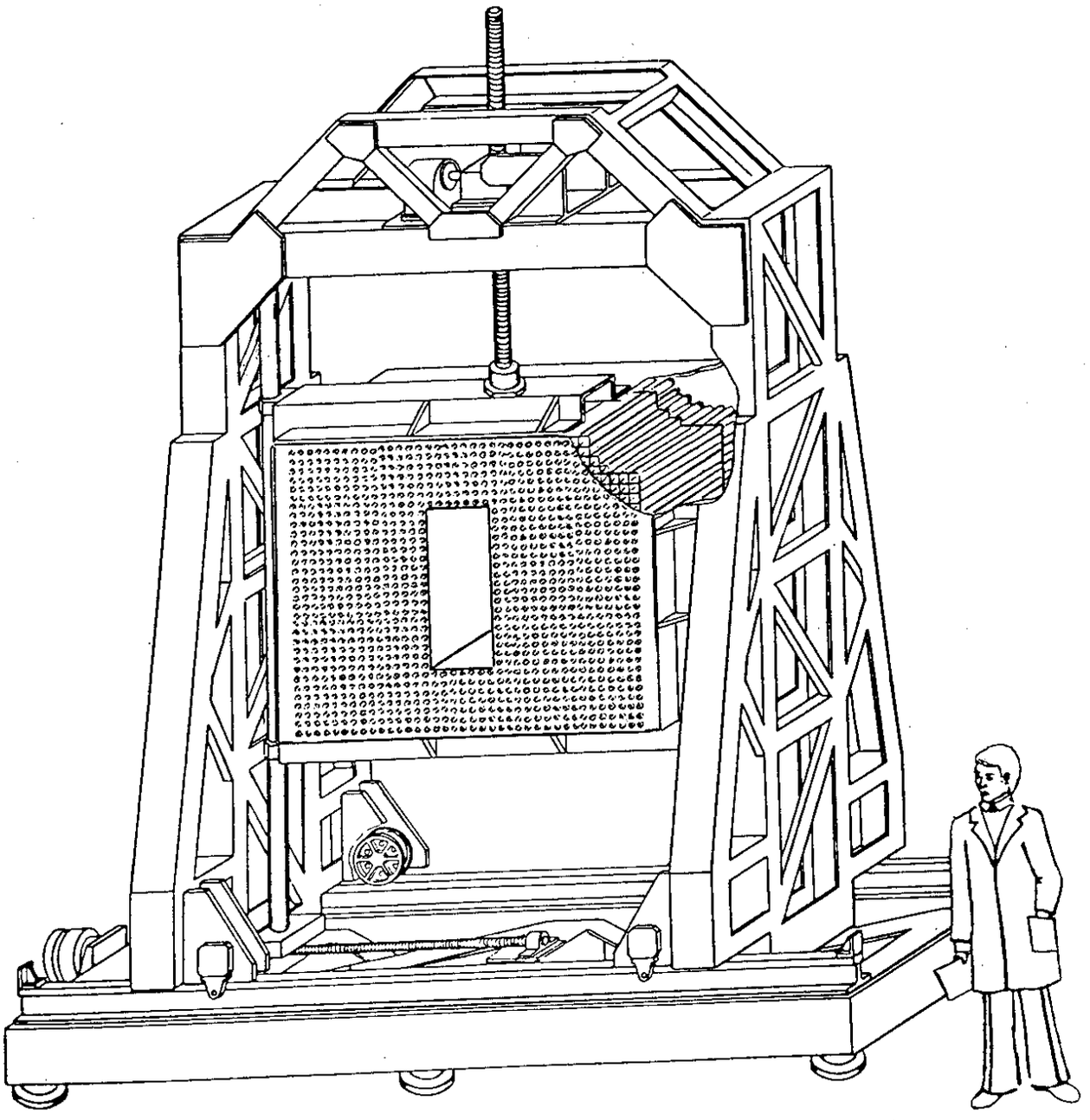

FIG. 7

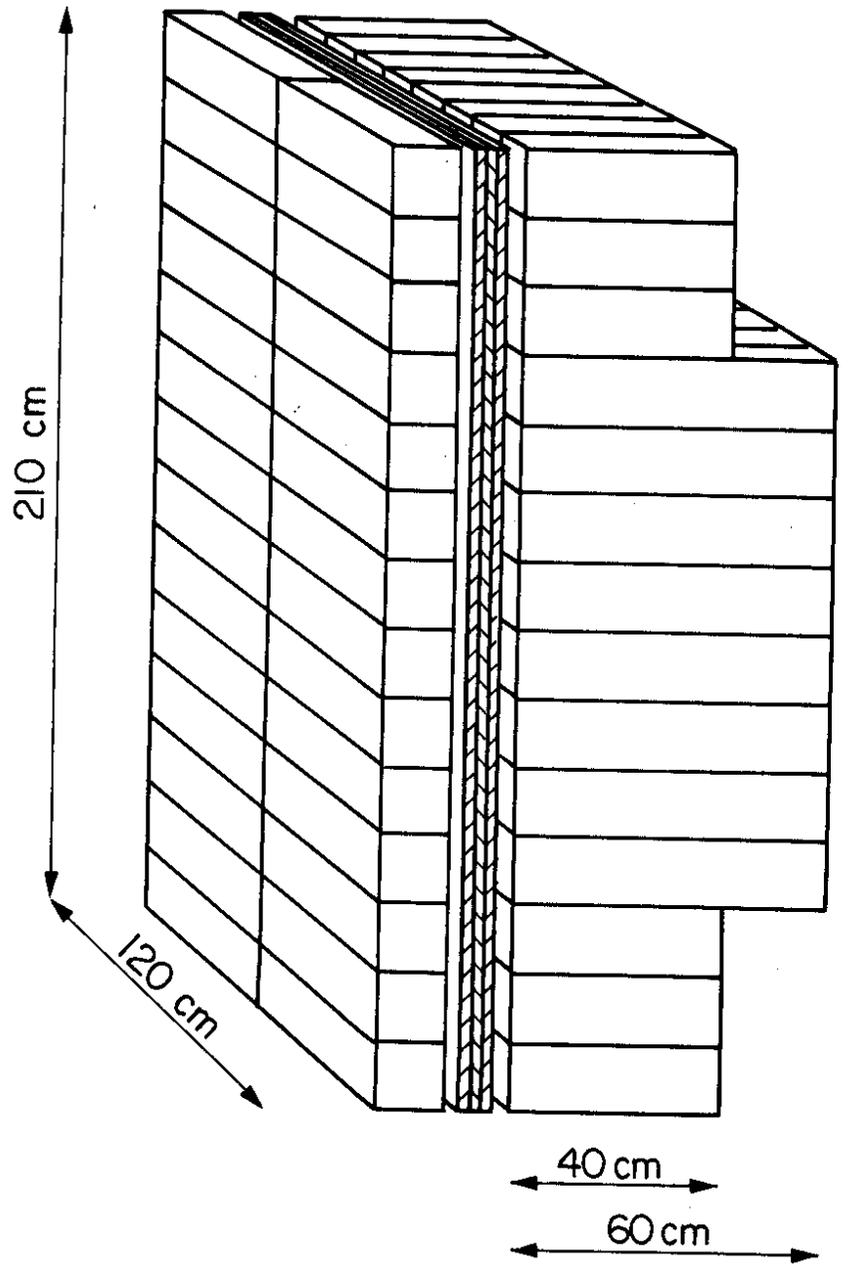
210 cm
120 cm
40 cm
60 cm
LEAD-GLASS CONVERTER WALL
THREE SCINT. HODOSCOPES
LEAD-GLASS ABSORBER WALL

Fig. 8

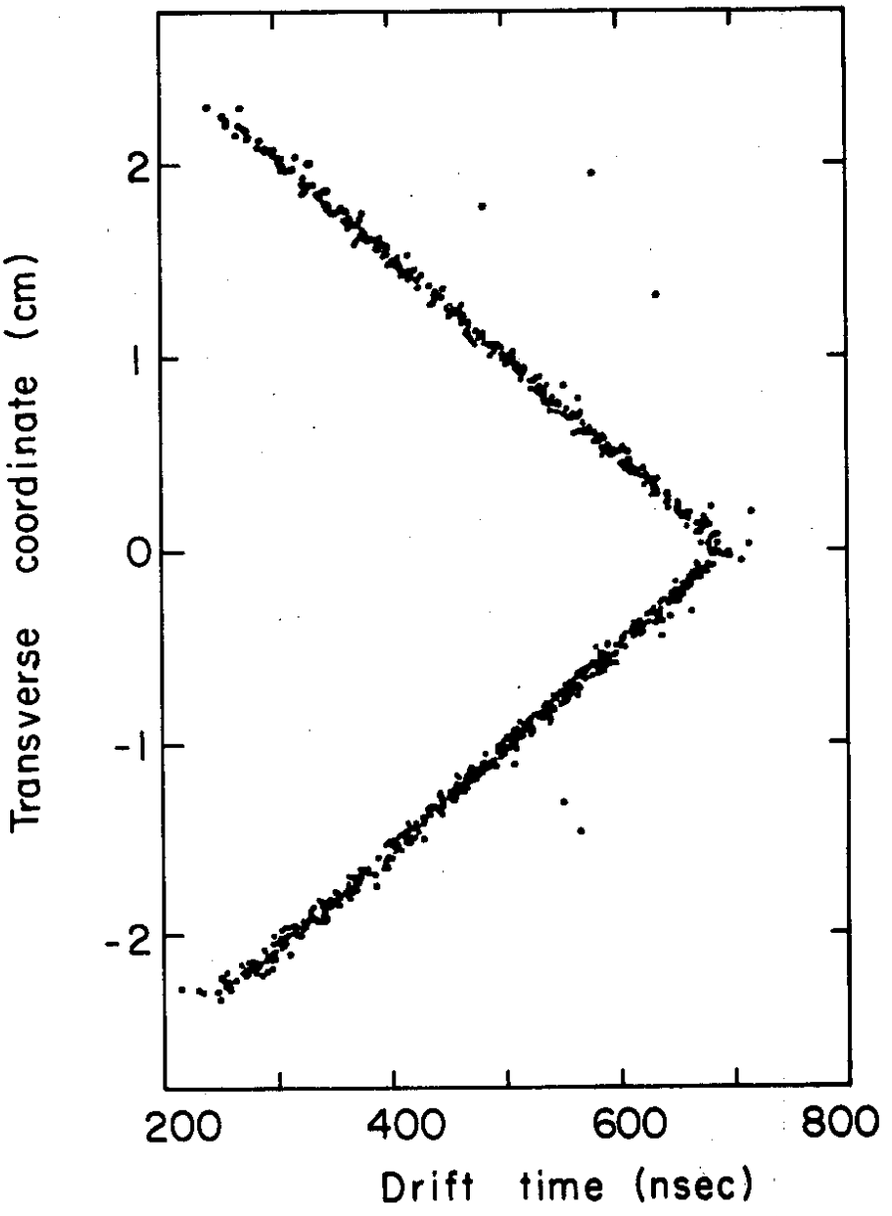
Transverse coordinate (cm)
2
1
0
-1
-2
200
400
600
800
Drift time (nsec)

FIG. 9

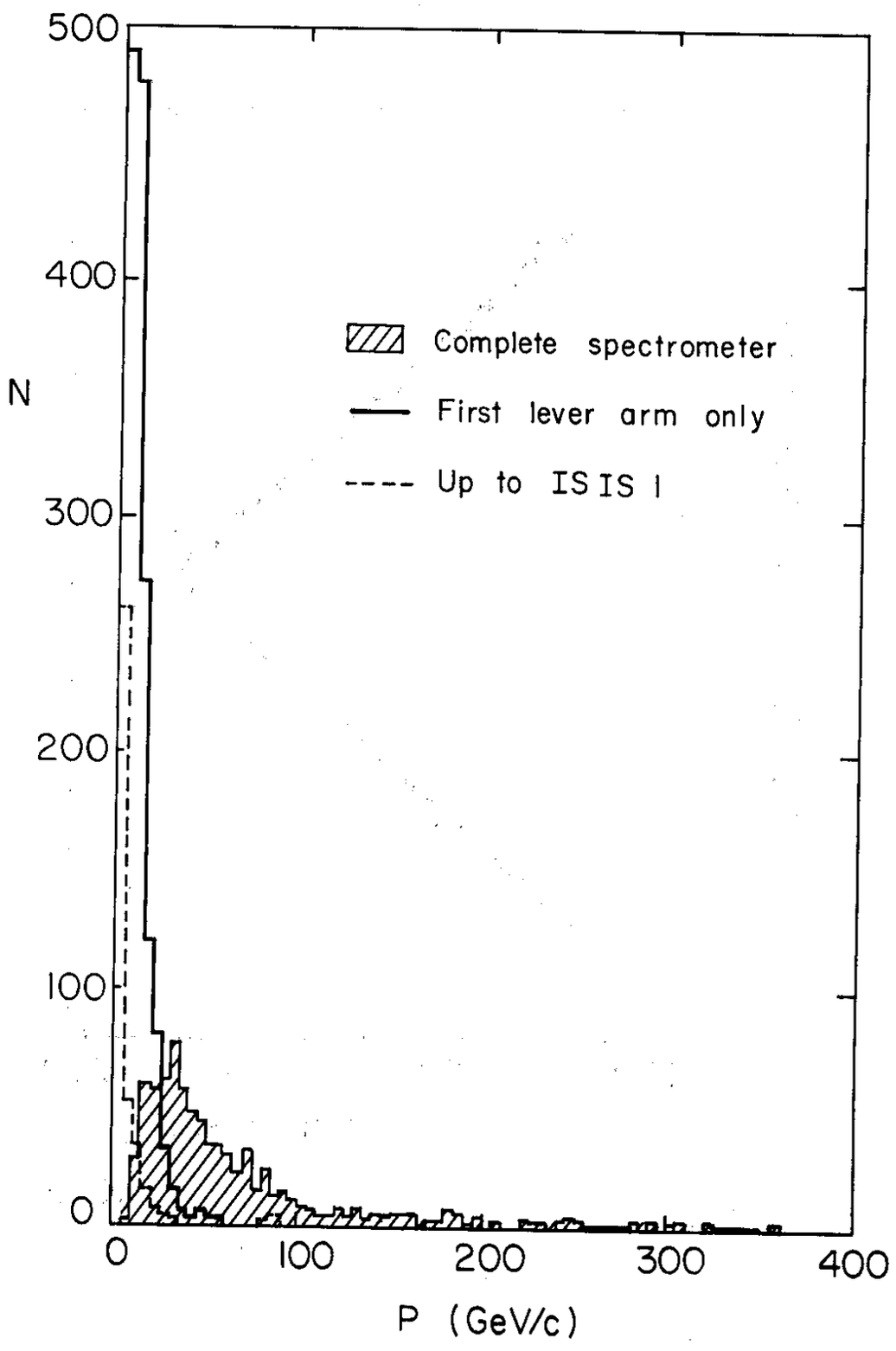
500
400
300
200
100
0
N
Complete spectrometer
First lever arm only
Up to IS IS I
0
100
200
300
400
P (GeV/c)

FIG. 10

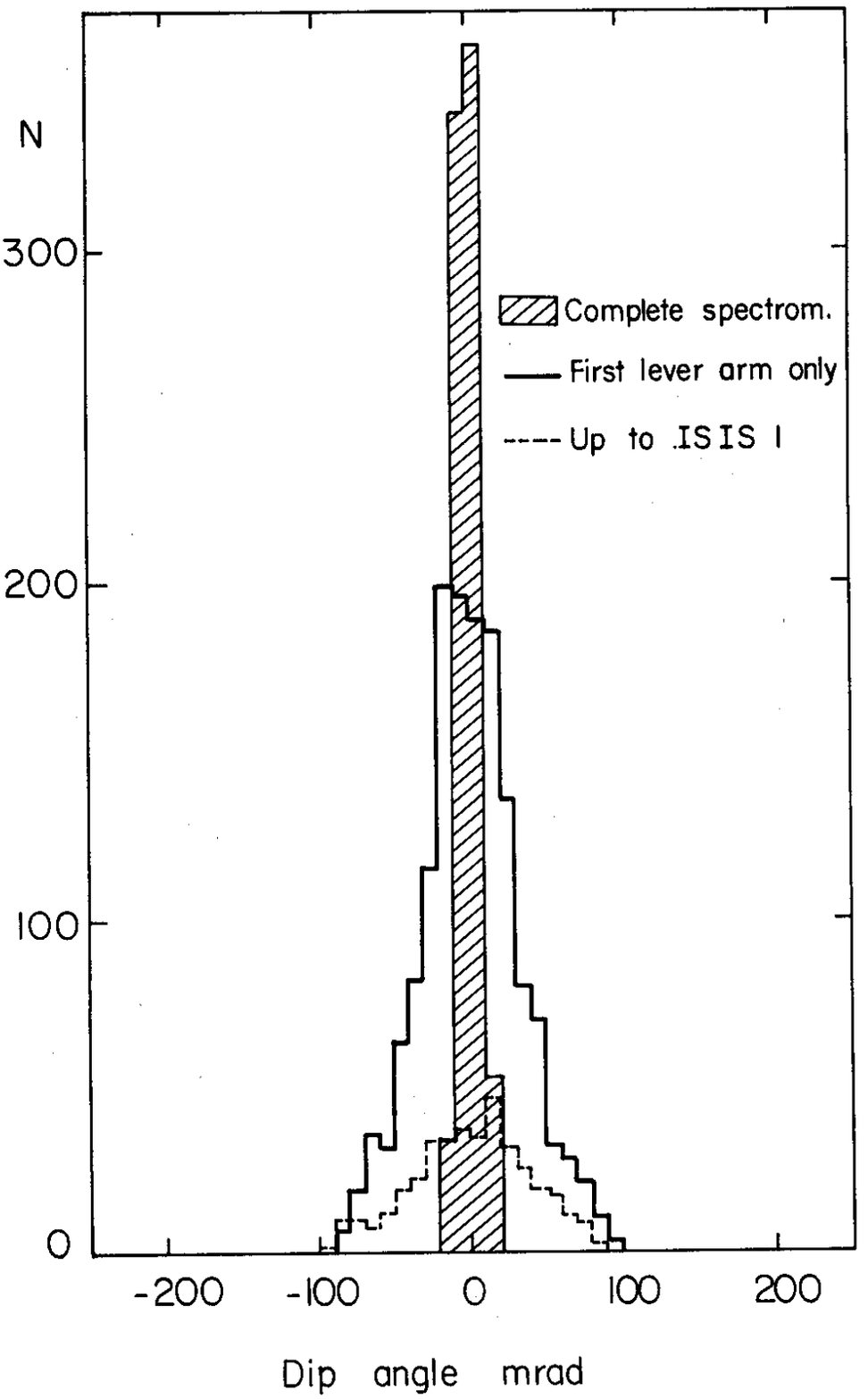
N
300
200
100
0
-200
-100
0
100
200
Complete spectrom.
First lever arm only
---- Up to .ISIS I
Dip angle mrad

FIG. II

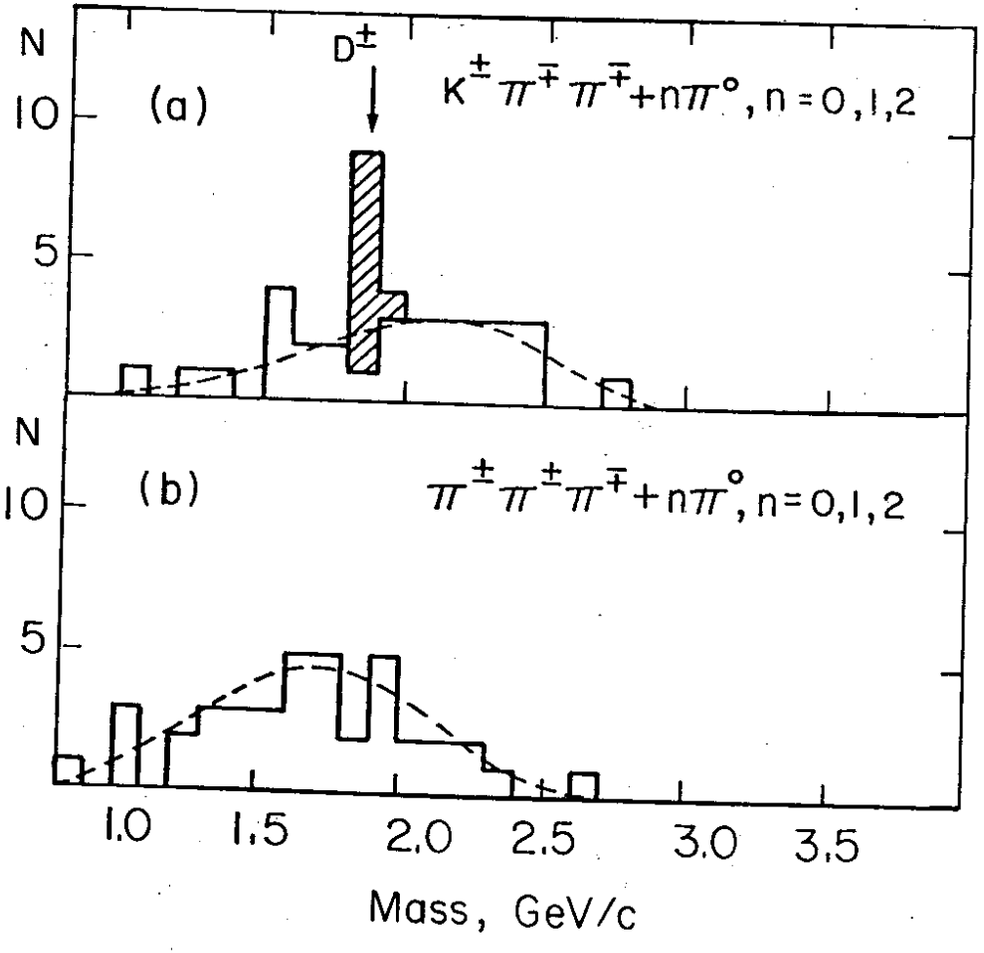
N
10
5
(a)
$D^{\pm}$
$K^{\pm}\pi^{\mp}\pi^{\mp}+n\pi^{\circ}$, n = 0, 1, 2
N
10
5
(b)
$\pi^{\pm}\pi^{\pm}\pi^{\mp}+n\pi^{\circ}$, n = 0, 1, 2
1.0
1.5
2.0
2.5
3.0
3.5
Mass, GeV/c

FIG. 12

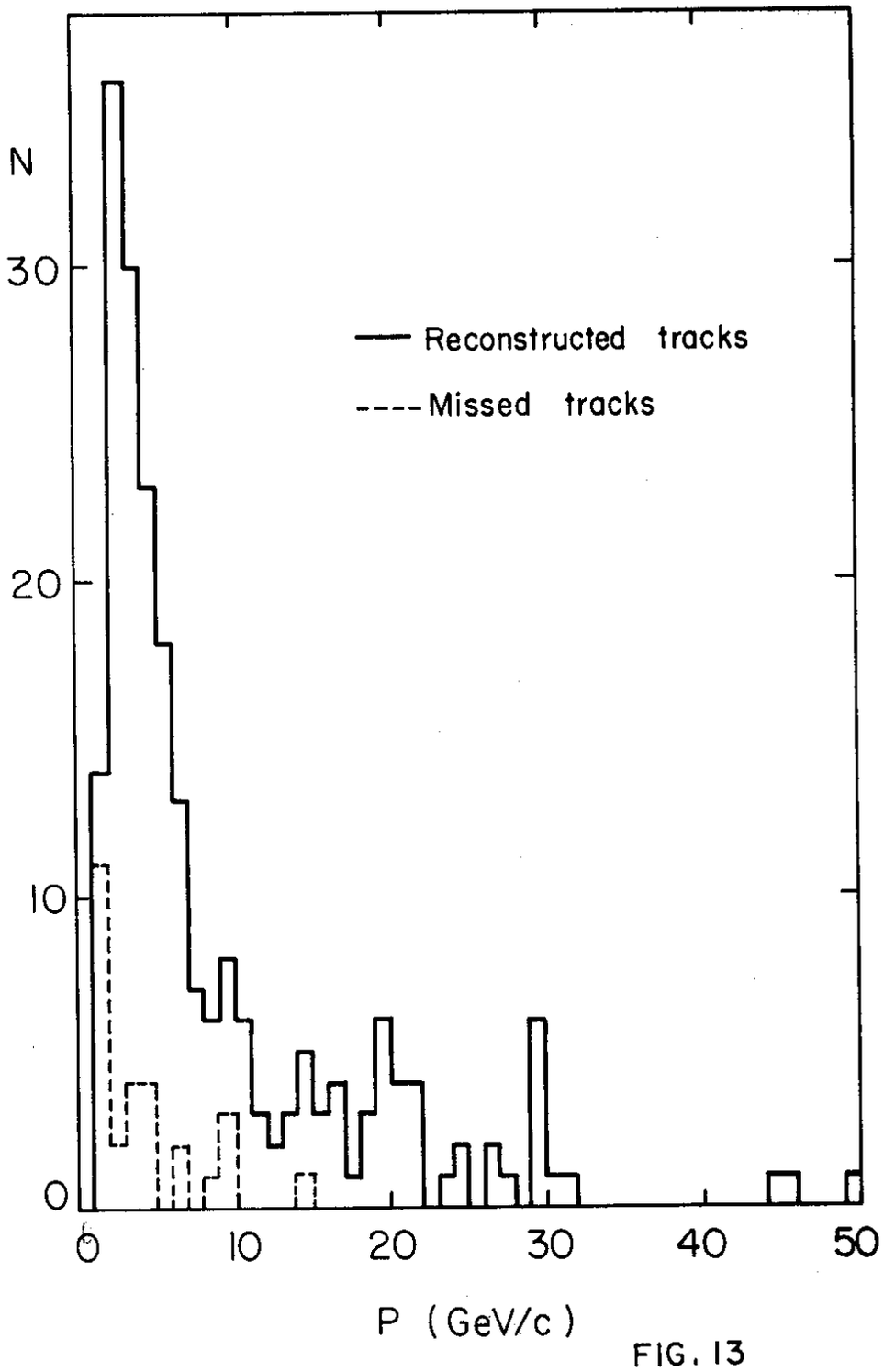
N
30
20
10
0
Reconstructed tracks
Missed tracks
0
10
20
30
40
50
P (GeV/c)

FIG. 13

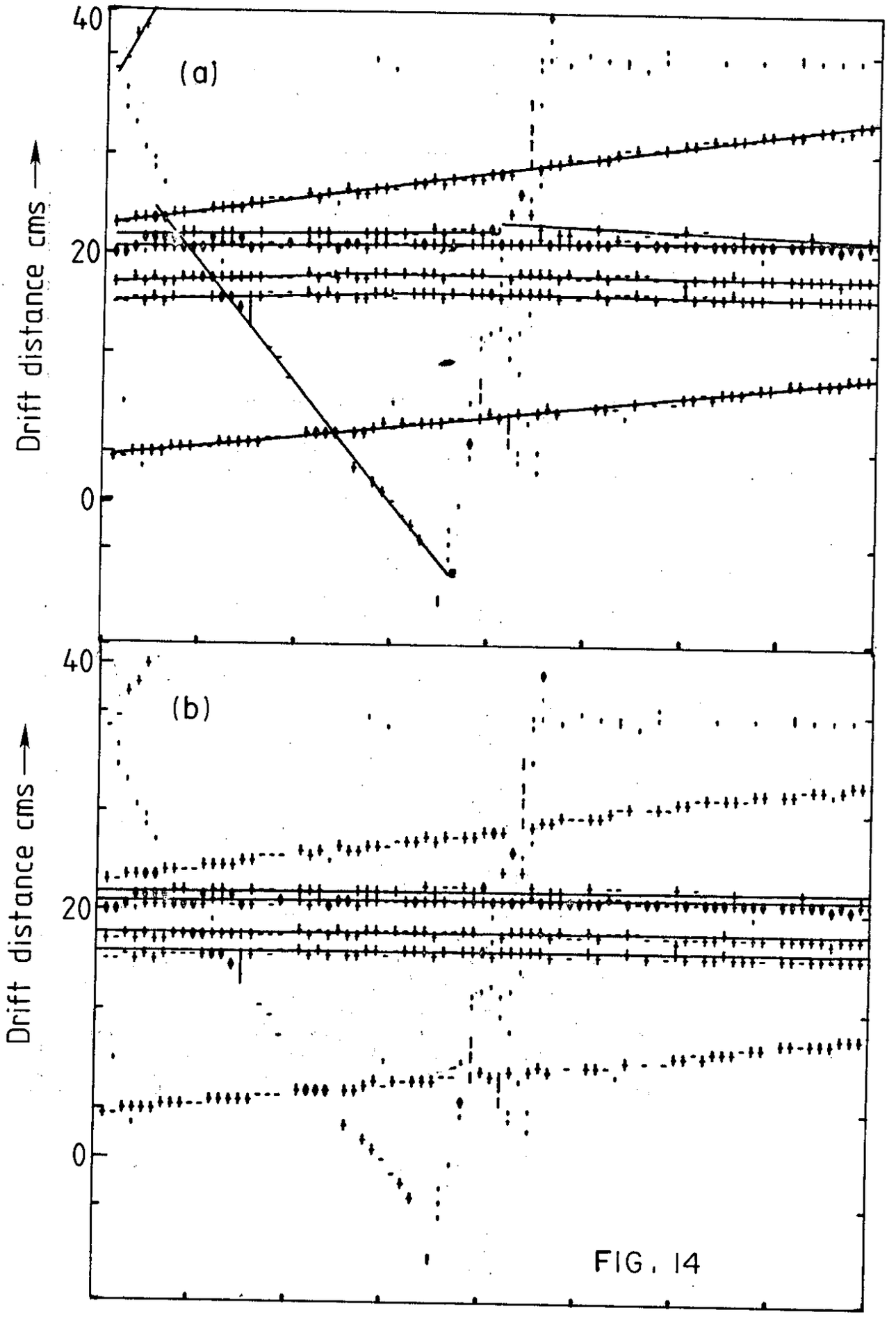

FIG. 14

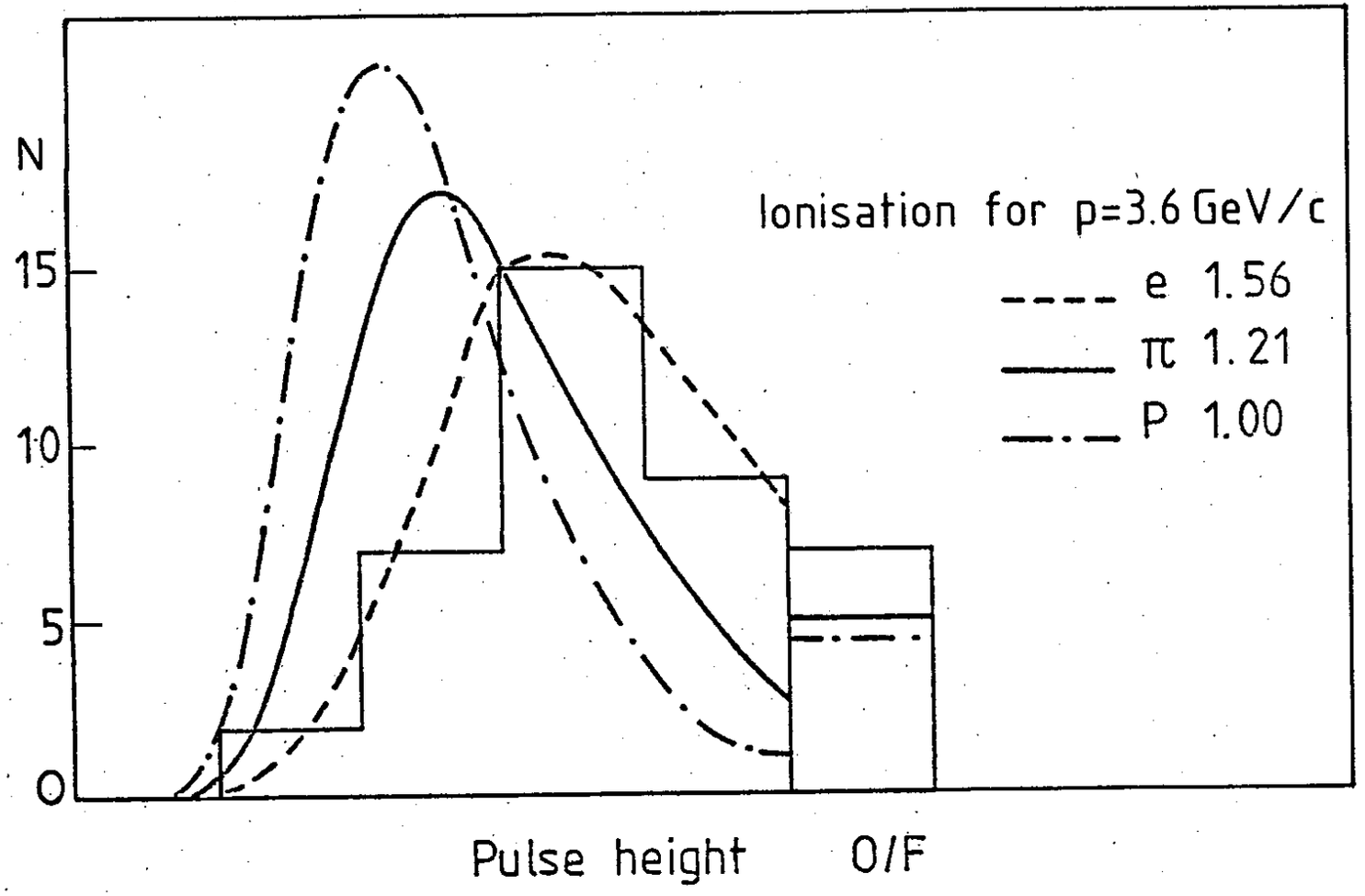
N
15
10
5
0
Ionisation for p=3.6 GeV/c
e 1.56
π 1.21
P 1.00
Pulse height
O/F

FIG. 15

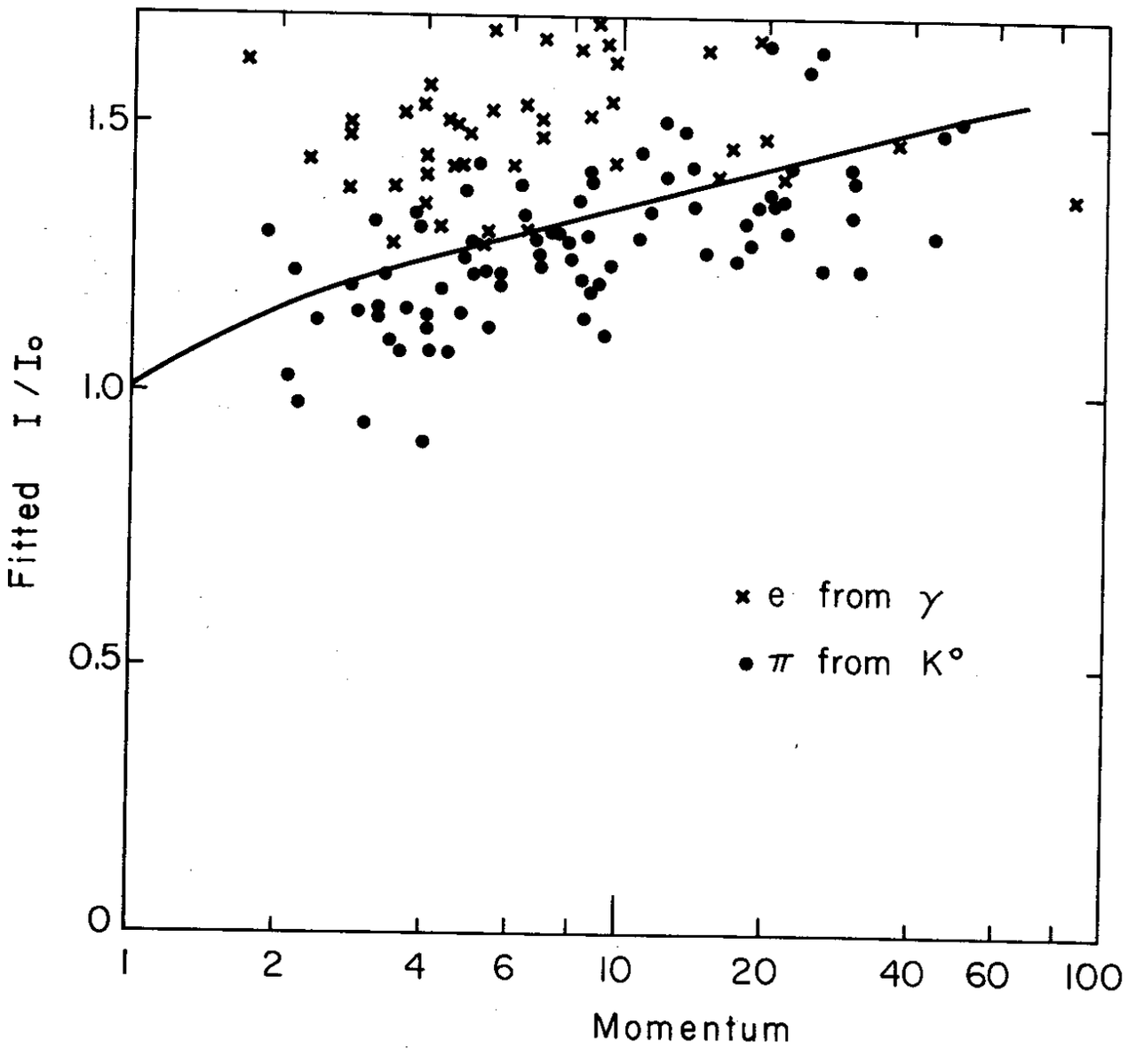
Fitted I / I₀
1.5
1.0
0.5
0
1
2
4
6
10
20
40
60
100
Momentum
× e from γ
• π from K°

FIG. 16

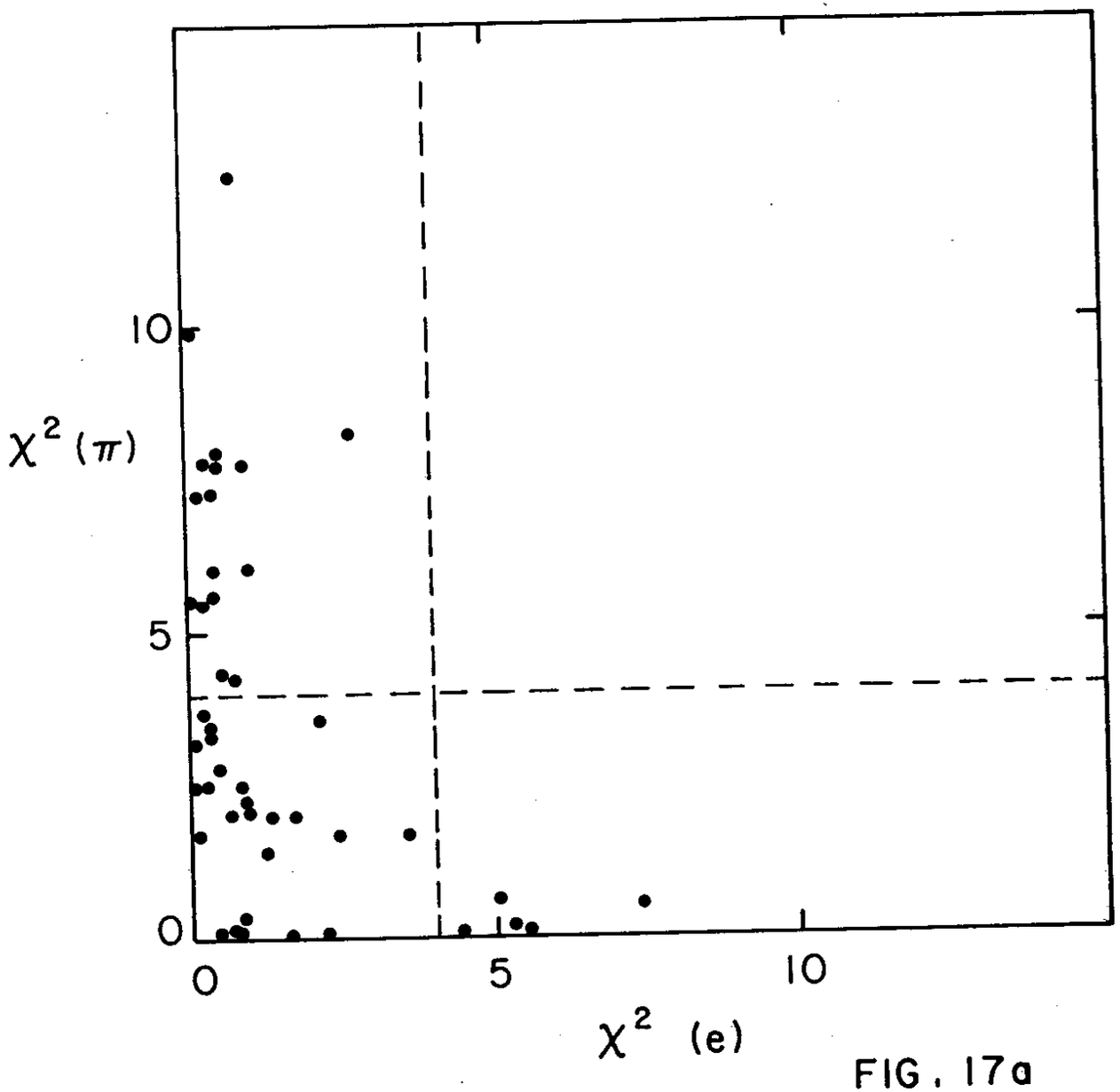

FIG. 17a

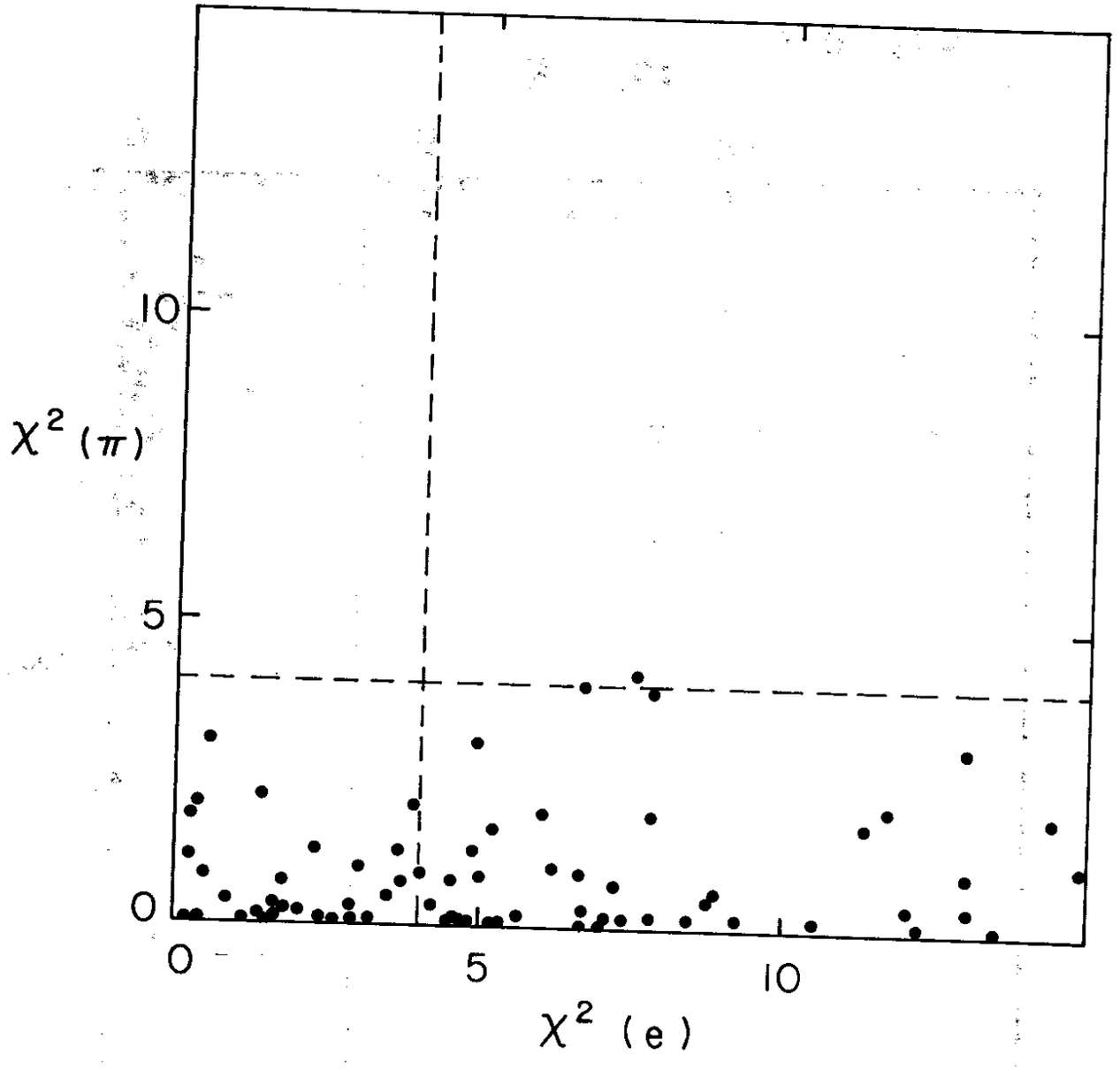

FIG. 17b

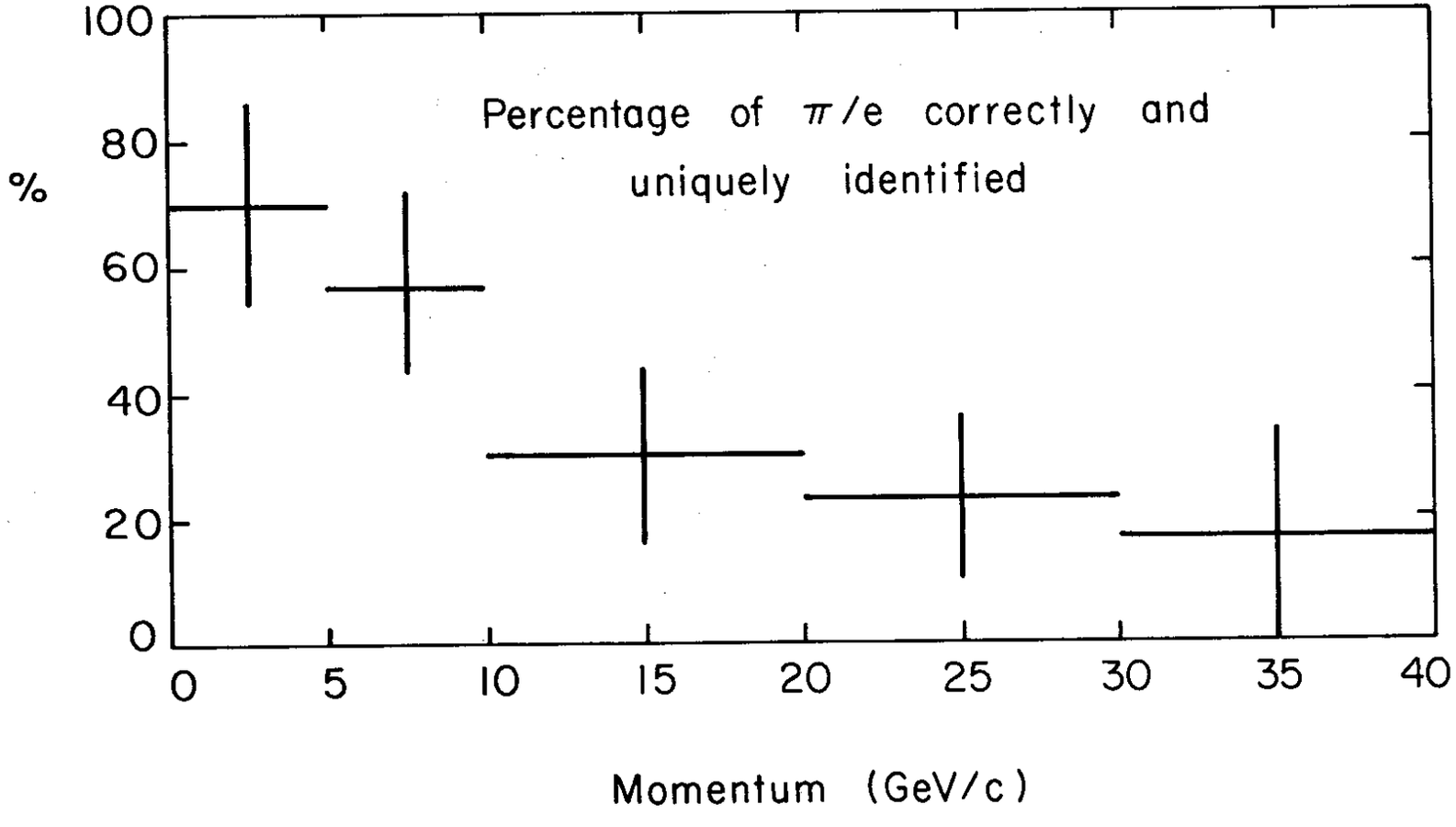
100
80
60
40
20
0
%
Percentage of π/e correctly and
uniquely identified
0
5
10
15
20
25
30
35
40
Momentum (GeV/c)

FIG. 18

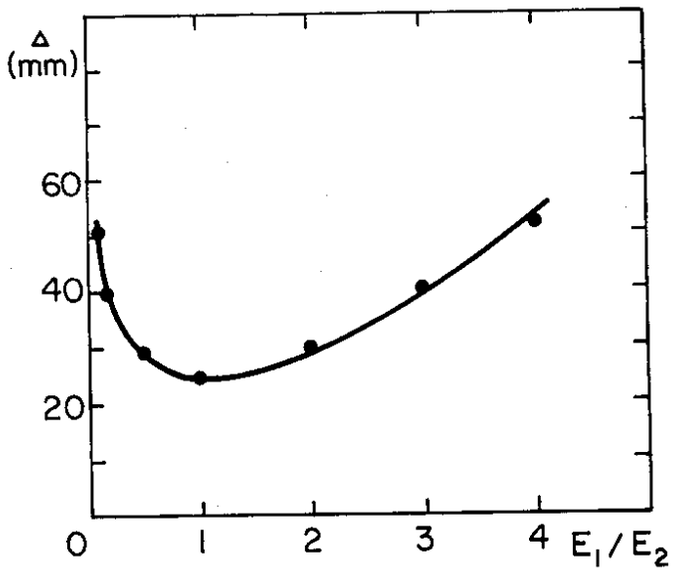

FIG. 19

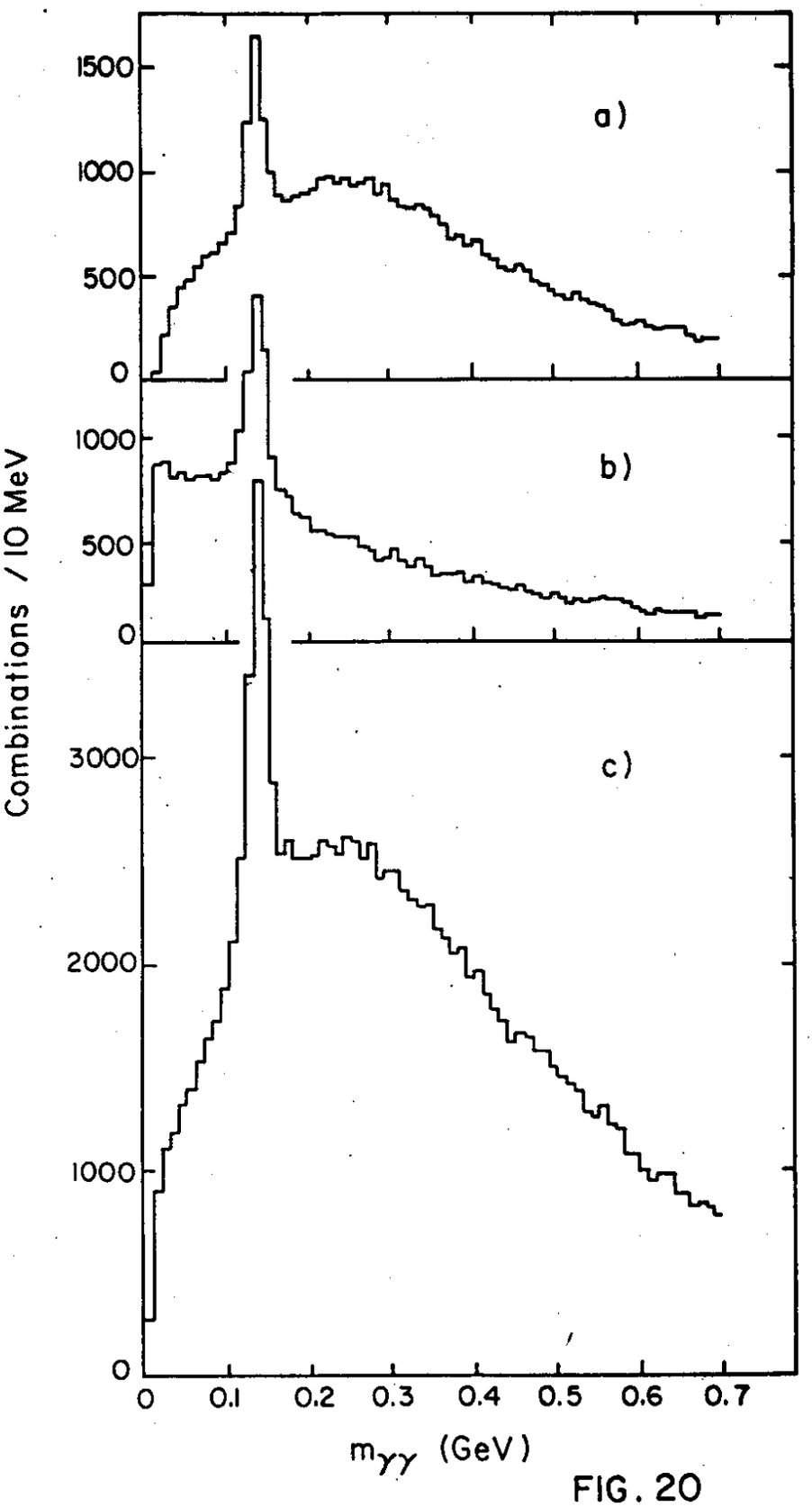
a)
b)
c)
1500
1000
500
0
1000
500
0
3000
2000
1000
0
0
0.1
0.2
0.3
0.4
0.5
0.6
0.7
Combinations / 10 MeV
$m_{\gamma\gamma}$ (GeV)

FIG. 20

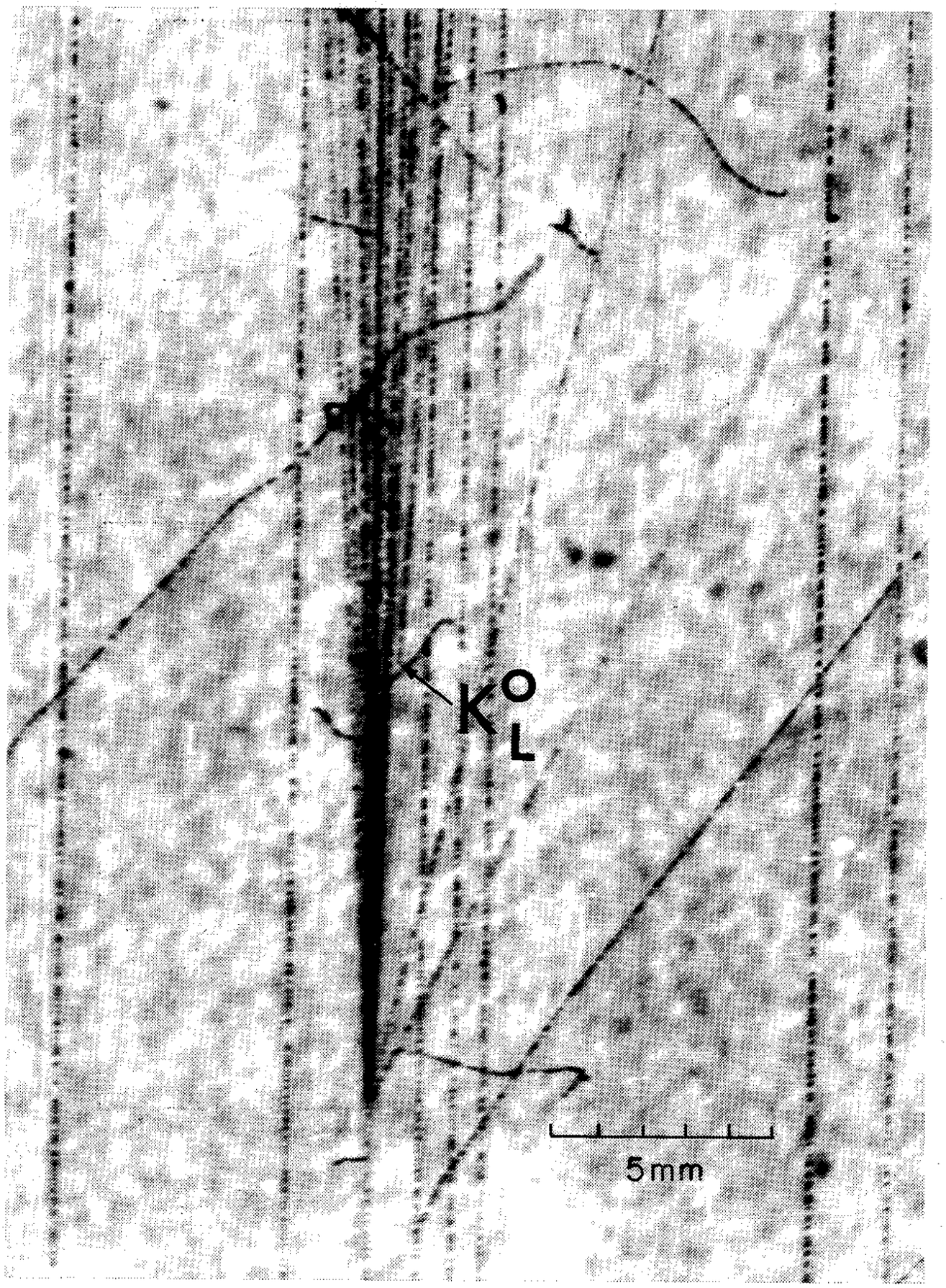

FIG. 21

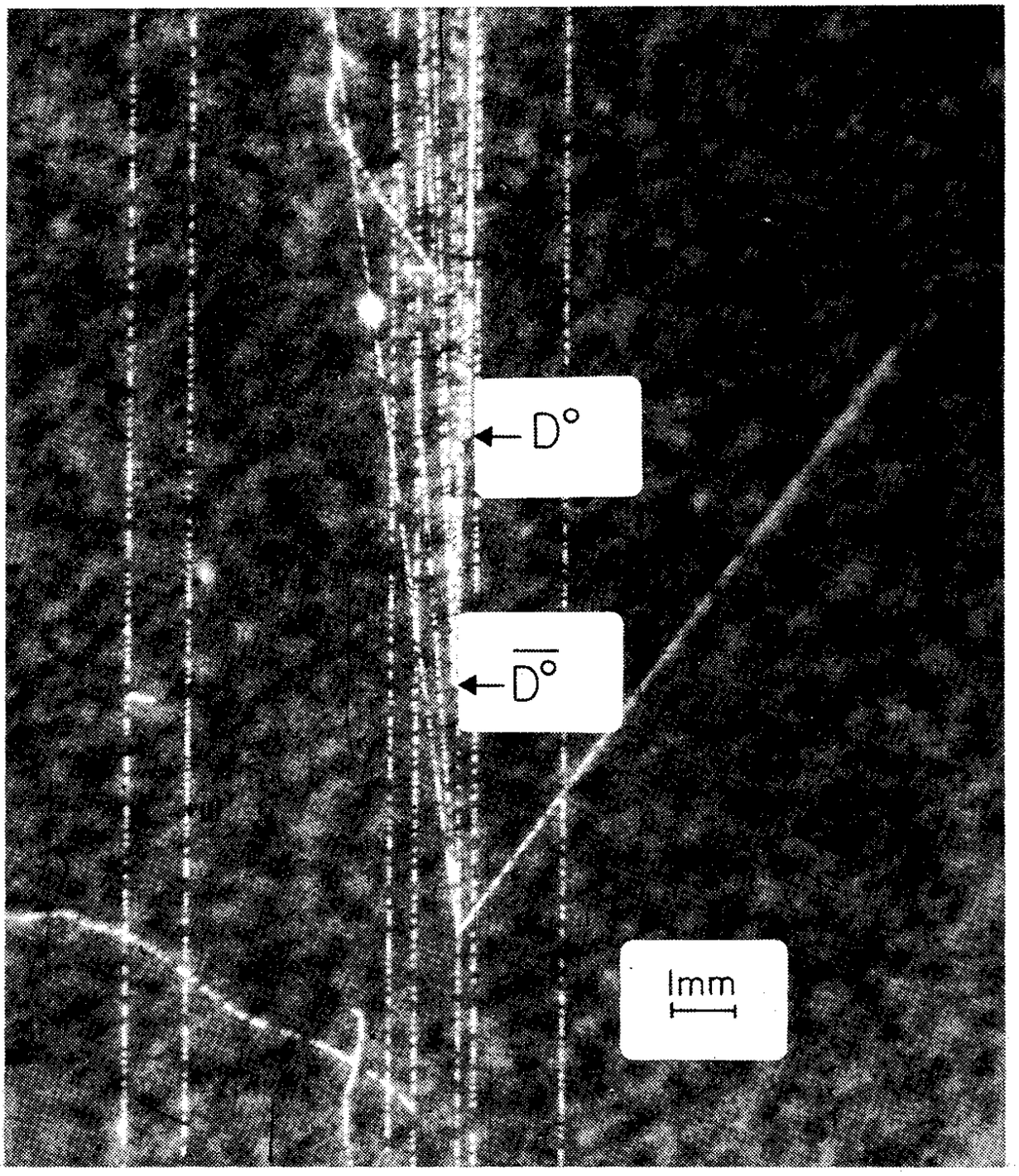

FIG. 22